Lack of an atypical PDR transporter generates an immunogenic *Cryptococcus neoformans* strain that drives a dysregulated and lethal immune response in murine lungs

Christopher J. Winski[1,#], Peter V. Stuckey[1], Armando M. Marrufo[1], Georgina Agyei[1,$], Robbi L. Ross[1,2,$], Tamanna Urmi[1,$], Sarah Chapman[5], and Felipe H. Santiago-Tirado[1,2,3,4,*]

[1] Department of Biological Sciences, University of Notre Dame, Notre Dame, Indiana, USA

[2] Integrated Biomedical Sciences, University of Notre Dame, Notre Dame, Indiana, USA

[3] Eck Institute for Global Health, University of Notre Dame, Notre Dame, Indiana, USA

[4] Warren Center for Drug Discovery, University of Notre Dame, Notre Dame, Indiana, USA

[5] Integrated Imaging Facility, University of Notre Dame, Notre Dame, Indiana, USA

Running Head: PDR transporter's role during cryptococcal infection

[#]Current address: Laboratory of Virology, National Institute of Allergy and Infectious Diseases, National Institutes of Health, Hamilton, MT, USA

[$]Equal contributions, name order determined alphabetically

*Address correspondence to Felipe H. Santiago-Tirado, fsantiago@nd.edu

Word Counts

Abstract: 236

Importance: 149

Text (excluding Methods, References, and captions): 6,785

23 **ABSTRACT**

24 *Cryptococcus neoformans* is an opportunistic fungal pathogen responsible for >150,000 deaths
25 every year with a mortality rate as high as 81%. This high medical burden is due, in part, to an
26 incomplete understanding of its pathogenesis. In a previous study, we identified a cryptococcal
27 atypical ATP-binding cassette (ABC) pleiotropic drug resistance (PDR) transporter, *PDR6*, that
28 affected antifungal resistance and host interactions. Here, we follow-up on the role of *PDR6* in
29 cryptococcal virulence. *In vivo*, mice infected with the *pdr6*Δ strain display altered
30 symptomatology and disease progression. Specifically, we observed a significant increase in the
31 innate immune cell populations in the *pdr6*Δ-infected mice when compared to their WT-
32 infected littermates. Furthermore, quantification of pulmonary cytokines/chemokines revealed
33 a robust increase of pro-inflammatory cytokines in mice infected with the *pdr6*Δ mutant strain.
34 Despite the documented sensitivity of the *pdr6*Δ strain to azole antifungal drugs, the treatment
35 of *pdr6*Δ-infected animals with antifungals did not affect survival, yet treatment with a
36 corticosteroid significantly extended survival, highlighting the importance of a
37 balanced/controlled host immune response. Results with mice that mount opposing immune
38 responses supports out hypothesis that the *pdr6*Δ strain induces a hyper-inflammatory immune
39 response, and that the mice succumb to immune-dependent tissue damage rather than the
40 fungal burden. This altered immune response is driven, in part, by changes in the mutant's
41 surface. Taken together, this study provides insights regarding cryptococcal pathogenesis and
42 highlights additional functions of PDR-type ABC transporters in pathogenic fungi.

43 **IMPORTANCE**

44 Yeasts of the *Cryptococcus* genus, especially *C. neoformans*, can cause disease with
45 unacceptably high mortality. This is due to delays in diagnostics, ineffective treatments, and an
46 incomplete understanding of the interactions between this fungus and our immune system. In
47 this study, we expand our knowledge of the biological function of the *PDR6* gene, particularly
48 its effect on modulating the host's immune response. Normally, *C. neoformans*'s infections are
49 characterized by an anti-inflammatory response that is unable to control the yeast. In the
50 absence of *PDR6*, the response to the infection is a dysregulated pro-inflammatory response
51 that initially controls the fungi but eventually results in death of the host due to too much
52 tissue damage. This is due, in part, to an altered fungal surface. Given the dual role of *PDR6* in
53 modulating antifungal sensitivity and immune responses, this work provides important insights
54 that may lead to new or improved therapeutics.

55 **INTRODUCTION**

56 Commonly associated with soil and bird guano, *Cryptococcus neoformans* is an
57 environmental, opportunistic yeast responsible for >194,000 infections every year (1). Upon
58 inhalation of spores or desiccated yeast, *C. neoformans* reaches the alveoli where it encounters
59 alveolar macrophages and other host immune cells (2); however, this fungus is capable of
60 establishing a unique intracellular niche that allows it to survive and replicate within these host
61 cells (3). Under certain immune conditions, this neurotropic fungus can then escape the lungs,
62 traverse the blood-brain-barrier, and enter the central nervous system (CNS), resulting in
63 cryptococcal meningoencephalitis (CME) with a mortality rate as high as 81% (1, 4, 5). Several
64 lines of evidence indicate that in addition to its use of host immune cells as replication havens,
65 *C. neoformans* can use infected cells as vehicles for dissemination and brain invasion (5, 6).
66 Hence, understanding this complex cryptococcal-phagocyte interaction from both fungal and
67 host perspectives represents a challenging but clinically relevant avenue of research given its
68 role in determining the course and outcome(s) of infection.

69 In addition to its ability to survive intracellularly, *C. neoformans* has several other
70 virulence factors including an antiphagocytic polysaccharide capsule that provides protection
71 from host stressors and masks several cryptococcal pathogen-associated molecular patterns
72 (PAMPs) including chitin, chitosan, mannoproteins, and β-glucans from host phagocytes (7). The
73 capsule, structurally composed of glucuronoxylomannan (GXM) and
74 glucuronoxylomannogalactan (GXMGal), is constitutively secreted/shed and is known to
75 modulate the host immune response in ways that promote infection (8). Additionally, *C.*
76 *neoformans* synthesizes cell wall-localized melanin that protects the yeast from ultraviolet

77 radiation and oxidative/nitrosative stress (9). Finally, the fungus displays thermotolerance, able
78 to grow at physiological-relevant conditions (37ºC + 5% CO_2) (10-12). These virulence factors are
79 integral to the pathogenesis of *C. neoformans* and as such, have been well-studied. However, *C.*
80 *neoformans* utilizes additional virulence factors which remain significantly understudied or
81 completely unknown. For example, we previously identified *PDR6* (also known as *AFR3*), a novel
82 ATP-binding cassette (ABC) transporter of the pleiotropic drug resistance (PDR) class, and
83 showed that it had a role in various cryptococcal virulence facets (13, 14). Present only in plants
84 and fungi, PDR transporters hydrolyze ATP to transport substrates across biological membranes
85 and have been primarily implicated in antifungal resistance (15, 16). Indeed, deletion of *PDR6*
86 (*pdr6*Δ) results in hyper-susceptibility to the azole-class of antifungals, but also showed *in vitro*
87 and *in vivo* defects in virulence. Thus, the role of *PDR6* in fungal pathogenesis and modulating
88 the host immune response warranted further investigation.

89 During microbial infections, the host's immune system is tasked with mounting an
90 appropriate and balanced immune response that will clear the infection while ideally limiting
91 tissue damage (17). An exaggerated Th1, or pro-inflammatory, response will likely clear a
92 microbial infection but also result in excessive cellular and tissue damage. Opposingly, an
93 inappropriate Th2, or anti-inflammatory, response will limit host damage but allow for
94 uncontrolled microbial proliferation and dissemination. Many pathogens take advantage of this
95 dichotomy to promote their infection. For example, early in HIV infection, this virus promotes
96 the secretion of pro-inflammatory cytokines IFN-γ and TNF-α, generating a strong Th1 response
97 that is permissive to viral replication (18, 19). In the context of *C. neoformans* infections, the
98 fungus promotes an anti-inflammatory Th2 response that allows for intracellular survival and

99 increased replication and dissemination, ultimately resulting in patient mortality (20, 21). It is
100 evident, however, that between these two immune response extremes, there is a whole
101 spectrum of responses to microbial infections, making this topic extremely complex but also an
102 important target for therapeutics. Hence, increased understanding of the immune response
103 against *Cryptococcus* can inform future therapeutic strategies where the immune response
104 could be modulated to benefit the host.

105 Our previous work characterizing *PDR6* showed that it had important roles in
106 cryptococcal biology and suggested that it was necessary for full virulence (13). Here, we study
107 the role of *PDR6* in the establishment and progression of disease using a murine inhalation
108 model of cryptococcosis. We show that a lower inoculum or treatment with antifungal drugs,
109 significantly decreased *pdr6*Δ fungal burdens, but do not change the outcome of the infection
110 by this mutant. Instead, the survival studies and immunological analyses suggest that the *pdr6*Δ
111 mutant elicits an altered host immune response characterized by significant increases in pro-
112 inflammatory cytokines, chemokines and innate immune cells. We treated the *pdr6*Δ-infected
113 mice with a corticosteroid and significantly extended their survival despite little to no change in
114 fungal burden. Moreover, using mouse breeds that are known to establish opposing immune
115 responses, we show that indeed the host's immune response is the main determinant of the
116 *pdr6*Δ infection outcome. This dysregulated immune response might be a consequence of
117 fungal surface alterations that expose antigenic and immunogenic components that normally
118 would be hidden from the immune system. Collectively, this study furthers our understanding
119 of cryptococcal pathogenesis, highlights the clinical importance of the host immune response in

120 controlling fungal infections, while also providing novel functions and insights of fungal PDR-
121 type transporters in the context of disease progression.
122
123 **RESULTS**
124 ***pdr6*Δ-infected mice succumb to infection despite decreased inoculum and fungal burden.** In
125 our previous study we determined that *PDR6* was required for complete cryptococcal virulence
126 as mice infected with the *pdr6*Δ mutant lived significantly longer and had decreased fungal
127 burdens when compared to their H99-infected littermates (13). Consistently, this finding was
128 recapitulated by *Oliveira et al.* using the *Galleria mellonella* invertebrate infection model (14).
129 Notably, the *pdr6*Δ-infected animals displayed altered symptomatology compared to their H99-
130 infected littermates. Specifically, at endpoint, the WT-infected mice displayed altered behavior
131 associated with neurological deficiencies, traditional of cryptococcal meningitis; in contrast, the
132 *pdr6*Δ-infected mice exhibited respiratory symptoms characterized by rapid and labored
133 breathing, suggestive of pneumonia. We hypothesized that the altered symptomatology could
134 be explained, in part, by differences in the establishment and progression of disease.
135 Previously, fungal burdens were only quantified at time of death (TOD), potentially overlooking
136 differences earlier on in the infection. To obtain a comprehensive view of the infection over
137 time, we inoculated mice with 5 x 10^4 cells of H99 or *pdr6*Δ strains, and quantified fungal
138 burden every seven days over the course of the infection (Fig. 1A). Interestingly, we found that
139 at 7 days post infection (dpi) there were no differences in the fungal burdens between the H99
140 and *pdr6*Δ-infected animals in all organs tested, suggesting that the strains established infection
141 similarly. Following this initial establishment, however, at 14 dpi there was a significant

142 decrease in fungal burden for the *pdr6*Δ strain compared to the WT. At 17 dpi, the H99-infected
143 mice succumbed to the infection with average lung, brain, and spleen burdens of 3.7 x 10^8, 1.9 x
144 10^6, and 1.3 x 10^4 CFU while the *pdr6*Δ-infected mice CFUs were 3.6 x 10^7, 5.1 x 10^3, and 677,
145 respectively. Between 14 and 28 dpi, the fungal burden of the *pdr6*Δ-infected animals remains
146 relatively constant in the brain and spleen, with a gradual, although small, increase in the lungs.
147 Then, after 28 dpi, there are gradual increases in all organs with final average CFU counts of 5.5
148 x 10^7, 1.1 x 10^5, and 1.5 x 10^3 in the lungs, brain, and spleen, respectively. The differences in
149 CFUs highlight key differences between H99 and *pdr6*Δ disease progression and suggests a
150 potential role of the adaptive immune response given the changes at 14 dpi.

151 Experimentally, the mice in our previous studies were inoculated with 5 x 10^4 cells, a
152 common inoculum for the murine inhalation model of cryptococcosis. Given the *in vitro* defects
153 of the *pdr6*Δ strain (13), and the fact that initially, the mice were able to control the infection
154 (Fig. 1A), we hypothesized that by lowering the fungal inoculum, the survival of the *pdr6*Δ-
155 infected mice would be extended with a potential for complete clearance of the infection. To
156 assess this, we decreased the initial inoculum 10-fold and infected mice with 5 x 10^3 cells and
157 monitored survival (Fig. 1B). The H99-infected mice had a mean survival of 21 days and the
158 *pdr6*Δ-infected mice displayed a mean survival of 36 days, similar to our studies with 10-fold
159 higher inoculum. Quantification of the fungal burden showed similar CFUs in all organs
160 between the animals infected with low and high WT inoculum (Fig. 1C compared to 1A);
161 however, despite having similar lungs CFUs, the animals infected with low *pdr6*Δ inoculum had
162 lower brain and spleen CFUs at TOD relative to the higher inoculum (Fig. 1C compared to 1A).
163 Evidently, using a lower inoculum did not change the trend we have seen before: the *pdr6*Δ-

164 infected mice still survive longer with significant decreases in fungal burden across all organs.
165 However, notably, in the *pdr6*Δ-infected mice the lower inoculum results in lower overall organ
166 burdens, with less dissemination, yet the *pdr6*Δ-infected mice still succumbed to the infection
167 with the same dynamics as when using a higher inoculum (35-38 days; Fig. 1B).
168
169 **Infection with *pdr6*Δ results in increased tissue damage.** Despite initially colonizing the
170 pulmonary environment, the *Cryptococcus*-associated fatal pathology occurs in the brain due to
171 the meningoencephalitis (22, 23). The altered symptomatology coupled with the differential
172 disease progression suggests that the *pdr6*Δ strain likely affects the host immune response.
173 Furthermore, when performing the previous fungal burden experiments, we observed
174 significant phenotypic differences in lung sizes in H99 v. *pdr6*Δ-infected mice (Fig. 2). To
175 qualitatively assess any potential differences at the cellular and tissue level, we harvested the
176 lungs of mock, H99, and *pdr6*Δ-infected mice, stained with hematoxylin and eosin (H&E), and
177 assessed tissue damage (Fig. 2 and Table 1). At 14 dpi, the gross anatomical images clearly show
178 increased size and inflammation of the H99-infected lungs when compared to the *pdr6*Δ-
179 infected. Additionally, the 10X and 40X images display deterioration of the lung parenchyma
180 and infiltration of *C. neoformans* which is not observed in the *pdr6*Δ-infected lungs (Fig. 2A). At
181 35 dpi, the *pdr6*Δ-infected lungs are severely inflamed, infiltrated with yeast, and characterized
182 by the presence of many inflammatory immune cells in the peri-bronchial and perivascular
183 space (Fig. 2B). Table 1 provides a quantitative summary comparing the H99 and *pdr6*Δ-infected
184 pulmonary tissue over time. Consistent with our observations in the fungal burden
185 experiments, there were little to no differences at 7 dpi. However, at 14 dpi the *pdr6*Δ-infected

186 lung contains the yeast in granuloma-like regions and have 30% less *C. neoformans* than the
187 WT-infected tissues. Furthermore, an increase in lymphocytes is observed in the *pdr6*Δ-infected
188 lungs relative to WT (105 to 26, respectively; Table 1). Finally, as the *pdr6*Δ-infected mice
189 approach TOD, the fungal infiltration, inflammation, and number of inflammatory immune cells
190 in the lung tissue all increase to levels well above those observed in the WT-infected animals at
191 TOD. Altogether, these findings suggest that the *pdr6*Δ strain elicits a differential immune
192 response in the pulmonary environment thus affecting disease progression and
193 symptomatology.
194
195 **Fluconazole treatment improves fungal burden but not outcome in *pdr6*Δ-infected mice.**
196 Currently, there a very few antifungal drugs available to treat cryptococcal infections and the
197 compounds that are available are either not effective, extremely expensive, or associated with
198 deleterious side effects (24). Fluconazole (FLC), a fungistatic azole class antifungal, is the
199 mainstay treatment option in low-resource regions where cryptococcal infections are endemic.
200 Mechanistically, FLC inhibits lanosterol 14α-demethylase, an enzyme in the ergosterol
201 biosynthesis pathway encoded by *ERG11* (25). In our previous study, we showed that the
202 deletion of *PDR6* increased the susceptibility of *C. neoformans* to azole class antifungals
203 including FLC (13). Given this phenotype, we hypothesized that treatment of *pdr6*Δ-infected
204 mice with FLC would result in total clearance of the infection, preventing the lethal immune
205 pathology. To test this, mice infected with either the WT or *pdr6*Δ strains, or mock infected,
206 were treated daily (starting 1 dpi) with either a low (8 mg/kg) or high dose (16 mg/kg) of FLC
207 and monitored for survival (Fig. 3A). The FLC treatment significantly extended survival in both

208 the H99 and *pdr6*Δ-infected animals compared to the untreated controls, albeit to the same
209 extent. Numerically, the mean survival for the untreated H99-infected mice was 17 days and
210 the low and high doses extended survival 4.5 and 6 days, respectively. Similarly, the mean
211 survival for the untreated *pdr6*Δ-infected mice was 34 days and the low and high doses
212 extended survival 5 and 7 days, respectively. Surprisingly, although the survival was similarly
213 extended between strains, quantification of the fungal burden revealed significant differences
214 (Fig. 3B-G). At 14 dpi, both doses of the FLC treatment significantly decreased the fungal burden
215 in the lungs, brain, and spleen only in the *pdr6*Δ-infected mice (Fig. 3B-D). Similarly, at TOD, the
216 daily FLC treatment resulted in an additional substantial decrease in the fungal burden of the
217 *pdr6*Δ-infected mice across all three organs, with several mice where the brain and spleen CFU
218 counts were below the limit of detection (LOD) (Fig. 3E-G). Not surprisingly, neither of the FLC
219 doses had a significant effect on WT-infected mice. This observation is interesting because
220 despite significantly decreasing the fungal burden with the FLC treatment, the *pdr6*Δ-infected
221 animals still succumbed to the infection.

222 To understand how the FLC treatment was affecting the pulmonary environment, we
223 prepared slides and performed qualitative histological analysis at TOD for both WT and *pdr6*Δ-
224 infected mice (Fig. 4 and Table 2). The H99-infected lungs at 14 dpi treated with FLC displayed
225 similar features to the previously pictured H99 untreated lungs, namely a high percentage of
226 fungal infiltration and tissue breakdown. In contrast, there was a clear decrease in fungi in the
227 FLC-treated *pdr6*Δ-infected lungs at this timepoint. Consistently, the FLC-treated *pdr6*Δ-infected
228 lungs at 35 dpi appear to have the infection controlled in granuloma-like regions (Fig. 4, inset 2)
229 with widespread immune cell infiltration (Fig. 4, inset 1). Interestingly, despite reduced

230 pulmonary CFUs (Fig. 3 and Table 2) and decreased inflammation (Fig. 4 and Table 2), the
231 *pdr6*Δ-infected mice were still succumbing to the infection. Together, these data suggest that
232 the mice infected with the *pdr6*Δ-strain are not necessarily dying directly because of the *C.*
233 *neoformans* infection, but rather indirectly because of an inappropriate host immune response.
234
235 ***C. neoformans pdr6*Δ strain elicits a strong pro-inflammatory immune response.** During
236 microbial infections, the host's immune response ultimately determines the clinical outcome
237 (26). Ideally, a balanced Th1 pro-inflammatory and Th2 anti-inflammatory immune response
238 will allow for microbial clearance and subsequent tissue repair. Previous studies have
239 determined that *C. neoformans* skews the immune response towards a permissive anti-
240 inflammatory Th2 response, thus benefiting the yeast and allowing for fungal replication and
241 subsequent dissemination (27). Given our previous observations, we hypothesize that the
242 *pdr6*Δ strain is instead generating a strong pro-inflammatory immune response that is able to
243 control the infection initially, but also damaging large areas of pulmonary tissue. To assess this,
244 we quantified the secreted cytokines and chemokines profile in the lungs and brains of H99 and
245 *pdr6*Δ-infected mice at their respective TODs (Fig. 5 and Fig. S1). Interestingly, we found that
246 several of the pro-inflammatory cytokines are significantly upregulated in the *pdr6*Δ-infected
247 lungs relative to WT (Fig. 5A). Specifically, the production of IL-1α, IL-1β, and MIP-1β (CCL4) is
248 increased 13-fold, 25-fold, and 37-fold respectively, when compared to the lungs of the H99-
249 infected mice. Interestingly, the expression of IL-13 and IL-33, anti-inflammatory cytokines
250 associated with allergic diseases, where also statistically upregulated in the *pdr6*Δ-infected mice
251 relative to WT. A similar trend was observed in the brain, although relative to the pulmonary

252 tissues, it was more muted (Fig. 5B), with statistically significant upregulation of G-CSF and IL-3
253 relative to the H99-infected brain. This weakened expression of inflammatory cytokines in the
254 brain might be due to the decreased capacity of the *pdr6*Δ mutant to disseminate coupled with
255 the immune-privileged status of the CNS. During a typical cryptococcal infection, the expression
256 of anti-inflammatory cytokines and chemokines are increased thus generating a Th2 response,
257 however, in the context of an infection with the *pdr6*Δ strain, the secretion of pro-inflammatory
258 cytokines and chemokines is significantly increased resulting in a damaging Th1 immune
259 response.
260
261 **Corticosteroid treatment extends survival in *pdr6*Δ-infected mice.** Clinically, corticosteroids
262 like dexamethasone are prescribed to downregulate the immune system. Mechanistically,
263 these anti-inflammatory drugs function by suppressing the migration of neutrophils and
264 decreasing lymphocyte colony proliferation (28). The potential of dexamethasone as a
265 treatment strategy during cryptococcal infection was investigated in a clinical trial but was
266 prematurely concluded because of adverse effects and increased mortality (29, 30); however,
267 corticosteroids have been used successfully to treat CME-associated inflammatory disorders
268 such as postinfectious inflammatory response syndrome and immune reconstitution
269 inflammatory syndrome (IRIS)(22). Given the robust pro-inflammatory immune response
270 observed in the *pdr6*Δ-infected mice, akin to fatal IRIS in humans, we hypothesized
271 dexamethasone treatment would dampen the aggressive Th1 response resulting in fungal
272 clearance and improved survival. Experimentally, we infected mice with either the H99 or
273 *pdr6*Δ strain, or mock infected, and treated them daily (starting at 1 dpi) with either 0.3 mg/kg

274 dexamethasone or a dexamethasone and 16 mg/kg FLC combination and assessed survival (Fig.
275 6A). The H99-infected mice that received the dexamethasone treatment displayed a significant
276 reduction in survival (mean survival of 13 days vs 17 days) when compared to the untreated
277 H99 control, while the combo therapy restored survival to that of the untreated H99-infected
278 group (mean survival of 16 days vs 17 days). This result corroborates the corticosteroid finding
279 reported in the human clinical trial (29, 30). In terms of the *pdr6*Δ-infected mice, both the
280 dexamethasone alone and in combination with FLC significantly extended survival. Numerically,
281 the mean survival of the untreated *pdr6*Δ-infected control group was 34 days and was extended
282 to 55 and 58 days in the dexamethasone and combination treated groups, respectively. The
283 survival studies were stopped after 60 dpi because the remaining mice, including the mock-
284 infected receiving the daily dexamethasone treatment (not shown), appeared sick despite not
285 meeting endpoint criteria. We concluded that after two months of daily corticosteroid
286 injections the immune systems of the mice had been ablated resulting in their poor
287 appearances. Despite the dexamethasone treatment extending survival in the *pdr6*Δ-infected
288 animals, the fungal burdens were differentially affected over the course of the experiment (Fig.
289 6B-G). Specifically, at 14 dpi the addition of dexamethasone significantly decreased the fungal
290 burden in the lungs in both the H99 and *pdr6*Δ-infected mice and little to no changes were
291 observed in either strain in the brain or spleen CFUs (Fig. 6B-D). At TOD the dexamethasone
292 treatment in the *pdr6*Δ-infected animals significantly increased the lung CFUs and the
293 combination therapy returned it to levels comparable to the untreated *pdr6*Δ-infected control
294 (Fig. 6E). Although not statistically significant, a similar trend was observed in the brain and
295 spleen of the *pdr6*Δ-infected mice (Fig. 6F & G). These effects were not seen in the WT-infected

296 mice. The dynamic changes in fungal burdens in the lungs of the dexamethasone and
297 combination treated *pdr6*Δ-infected mice can be explained by the absence or lack of
298 inflammatory immune cells to control the infection and the addition of FLC lowers the CFUs as
299 the fungistatic nature of the antifungal is unable to clear the initial infection. Collectively, these
300 data further confirm and highlight the altered disease progression elicited by the *pdr6*Δ mutant
301 and, more importantly, demonstrate the positive clinical outcome associated with controlling
302 the inappropriate pro-inflammatory immune response.
303
304 **Combination dexamethasone and fluconazole treatment reduces pulmonary tissue damage in**
305 ***pdr6*Δ-infected animals.** Based on our previous results, it is evident that the addition of the
306 corticosteroid is benefiting the *pdr6*Δ-infected mice by significantly extending survival.
307 Histological analysis of the lung tissue at TOD for both WT and *pdr6*Δ-infected mice was
308 performed to visualize changes in fungal infiltration, tissue inflammation, and immune cell
309 recruitment (Fig. 7 and Table 3). Visually, the treatment with dexamethasone had a profound
310 effect given the qualitative reduction in inflammatory cells across all conditions. The lungs of
311 the H99-infected mice that received dexamethasone are not as inflamed as those from
312 untreated mice but the destruction of the lung tissue is devastating (Fig. 7A). The lack of
313 immune cells allowed for the uncontrolled proliferation of *C. neoformans* resulting in increased
314 damage of the pulmonary tissue. Similarly, the dexamethasone treated lungs of the *pdr6*Δ-
315 infected display intense fungal proliferation but there is qualitatively less damage when
316 compared to the H99-infected animals (Fig. 7B and Table 3). The combination dexamethasone
317 and FLC treatment reduced the fungal infiltration in both the H99 and *pdr6*Δ-infected mice

318 when compared to the dexamethasone alone (Fig. 8 and Table 4). In fact, despite the presence
319 of some yeast, the *pdr6*Δ-infected lung tissue appears relatively healthy with little to no
320 damage and inflammation suggesting that another mechanism may be responsible for the mice
321 reaching endpoint (Fig. 8B and Table 4).
322
323 ***pdr6*Δ-infected mice display an increase in innate immune cells populations.** During microbial
324 infections, the cells of the innate immune system represent the first line of defense which is
325 followed by the activation and recruitment of the adaptive immune response (31). In a *C.*
326 *neoformans* infection, lung macrophages represent the innate population primarily responsible
327 for initial clearance, although some recent literature suggests neutrophils also play a supportive
328 role (32-34). However, CME is an AIDS-defining disease, and low $CD4^+$ T-cell counts is a major
329 susceptibility for CME, indicating that the adaptive immune response also plays an important
330 role controlling cryptococcal infections (35). Provided the altered immune response to the
331 *pdr6*Δ strain, we expected alterations to both the quantity and the composition of innate and
332 adaptive inflammatory immune cells. To test this, we harvested leukocytes from the lungs of
333 H99 and *pdr6*Δ-infected mice at 14 dpi (close to TOD of WT-infected mice) and at 35 dpi (close
334 to TOD of *pdr6*Δ-infected mice) and quantified the different populations using flow cytometry
335 (Fig. 9 and Fig. S2). Quantification of the total innate immune cell populations at 14 dpi showed
336 that the FLC, dexamethasone, and combination treatments led to a significant decrease in the
337 *pdr6*Δ-infected animals whereas there were no significant changes in the H99-infected mice
338 (Fig. 9A). However, no reduction was observed when compared as a percentage of $CD45^+$ cells
339 (Fig. 9B), although, interestingly, a significant increase in the ratio of neutrophils and

340 macrophages was seen in the combination-treated *pdr6*Δ-infected mice (Fig. 9B). At this time
341 (14 dpi), quantification of the total adaptive immune cells showed a marked increase in the
342 *pdr6*Δ-infected animals when compared to their H99-infected counterparts, although only the
343 $CD8^+$ T-cells were statistically significant (Fig. 9C, untreated bars). Furthermore, all treatments
344 decrease the number of lymphocytes in the *pdr6*Δ-infected animals relative to the WT, specially
345 the $CD8^+$ T-cells (Fig. 9C, +FLC, +Dexa, and +Dexa +FLC bars). The same trend is observed when
346 compared as percentage of CD45+ cells (Fig. 9D). At 35 dpi there are some minor differences in
347 the adaptive immune cell populations when comparing the treated groups (Fig. 9G & H).
348 Interestingly, when comparing the untreated *pdr6*Δ-infected mice at 35 dpi with 14 dpi there is
349 a significant reduction in the total number of innate immune cells (Fig. 9D & H, untreated bars).
350 Moreover, a significant increase in macrophages is observed in the *pdr6*Δ-infected mice when
351 compared to the H99-infected (Fig. 9E & F, untreated bars). Using CD68 as a marker of
352 inflammatory macrophages in histological slices confirmed this influx of immune cells specific
353 for the *pdr6*Δ-infected (Fig. S3). Notably, the dexamethasone treatment (alone or with FLC) in
354 the *pdr6*Δ-infected animals significantly decreases the number of macrophages which is
355 replaced by a significant increase in the number of neutrophils (Fig. 9E & F, +Dexa and +Dexa
356 +FLC bars). It appears that in the absence of Pdr6, a robust and sustained macrophage response
357 is mediating the tissue damage, whereas in the WT-infected mice, neutrophils are the main
358 innate cells accumulating in the lungs. Collectively, these results showed that infection with the
359 *pdr6*Δ strain results in the increased recruitment of adaptive immune cells early on during the
360 infection while an increase in innate immune cells, specifically macrophages, was observed in

361 the later stages of the disease. This further explains the strong pro-inflammatory response,
362 altered disease progression, and differential symptomatology specific to the *pdr6*Δ strain.
363
364 **The magnitude of the host response to *pdr6Δ* strain infection influences the disease outcome.**
365 Up to this point, our results indicate that infection with the *pdr6*Δ strain results in the
366 recruitment of more inflammatory immune cells to the lungs, that initially can control the
367 infection but, when sustained over several weeks, leads to increased pulmonary damage and
368 mortality. This is supported by the dexamethasone treatment experiments, where dampening
369 the immune response significantly extended survival in the *pdr6*Δ-infected animals. However,
370 these experiments were done in the A/J mouse background, which is known to be "muted" in
371 response to cryptococcal infection. We wondered if the same would happen in mice that are
372 known to mount either strong pro-inflammatory (C57BL/6) or anti-inflammatory (BALB/c)
373 responses against WT *C. neoformans*. With C57BL/6 mice, we envisioned two potential
374 outcomes: the already skewed pro-inflammatory response of this mouse in combination with
375 the pro-inflammatory response induced by *pdr6*Δ could result in complete clearance, or
376 augment the tissue damage and result in hypervirulence. With the BALB/c mice, we had one
377 hypothesis: the strong anti-inflammatory response of this mouse could counter the pro-
378 inflammatory response induced by *pdr6*Δ enough to reach a balance, allowing for clearance or
379 latency. To test this, we infected either C57BL/6 or BALB/c mice with 5 x 10^4 cells of H99 or
380 *pdr6*Δ strains and followed their survival as before. Whenever a mouse reached humane
381 endpoints, organs were harvested for CFU and cytokine quantification. Interestingly, the
382 C57BL/6 survival curve was similar to the A/J curve (Fig. 10A), with a median survival time of 18

383 days for H99-infected mice and 42 days for *pdr6*Δ-infected mice, and decreased *pdr6*Δ burden
384 in all organs (Fig. 10B – D). Indeed, the cytokine profile of the *pdr6*Δ-infected C57BL/6 was a
385 more pronounced pro-inflammatory A/J profile, with the same upregulation of IL-1α, IL-1β, and
386 MIP-1β, but additionally, there was strong upregulation of IL-6, MIP-1α, and G-CSF (Fig. 10E and
387 Fig. S4). In contrast, 70% of the *pdr6*Δ-infected BALB/c mice survived to the end of the
388 experiment (60 dpi), whereas all of the H99-infected mice succumbed by day 18 (Fig. 10F).
389 Surprisingly, the surviving mice had fungal burdens higher than the H99-infected mice at TOD
390 (Fig. 10G – I), yet they showed no symptoms. Comparison of the immune profiles between
391 C57BL/6 and BALB/c showed expected similarities (IL-1α, IL-1β, and MIP-1α) but also clear
392 differences (lack of IL-6 and G-CSF signaling and stronger induction of IL-13 in BALB/c)(Fig. 10E
393 & J, and Fig. S4). Similarly to the dexamethasone treatment in A/J mice, the *pdr6*Δ-infected
394 BALB/c mice survived longer despite having higher fungal burdens, strongly suggesting that the
395 fatal pathology is driven by the immune response and not by the fungus.
396
397 ***C. neoformans pdr6Δ* strain exhibits altered PAMP exposure.** Experimentally, we have studied
398 the host response to this cryptococcal mutant but the question remains as to how is this
399 mutant modulating the immune system and generating a robust Th1 response. In our previous
400 work, we showed that *PDR6* encodes an atypical transporter localized to the endoplasmic
401 reticulum (ER) and plasma membrane (PM) involved in ergosterol trafficking (13). Others have
402 suggested a direct relationship between altered ergosterol levels and host immune responses
403 (36, 37) as well as altered surface composition due to defects in PM fluidity and lipid rafts (38,
404 39). We hypothesize that in the absence of *PDR6* there would be less ergosterol in the PM,

405 potentially resulting in downstream alterations to the cryptococcal surface that would expose
406 immunogenic components. To assess this, we grew H99 and *pdr6*Δ cells in YPD, stained with
407 fluorescent dyes that recognize and bind to fungal cell wall components, and visualized the cells
408 using microscopy. Under this condition, we did not observe any difference between the H99
409 and *pdr6*Δ stained cells (data not shown). However, previous studies have reported a
410 correlation between growth conditions and the architecture of the fungal cell wall (40). This led
411 us to repeat the experiment with cells grown under host-like conditions (DMEM at 37ºC + 5%
412 CO_2) (Fig. 11A). Under these conditions, the *pdr6*Δ strain displayed increase staining with
413 calcofluor white (CFW) and concanavalin A (ConA) suggestive of increased exposure of chitin
414 and mannoproteins, respectively. Similarly, there was some staining with the β-(1,3)-glucan
415 antibody suggestive of more exposed β-glucans in the *pdr6*Δ mutant (Fig. 11A). Despite the
416 differences observed microscopically, quantification of the staining intensity of these dyes, and
417 of eosin Y (EoY) which stains chitosan, using flow cytometry did not reveal statistically
418 significant increases in intensity in the *pdr6*Δ strain when compared to the H99 (Fig. 11B – E).
419 The positive control, *cap59*Δ, deficient in polysaccharide capsule synthesis and thus with
420 increased exposure of its cell wall, showed the expected increases in intensity. This was
421 confirmed using three independently made *pdr6*Δ mutants (Fig. 11B – E and Fig. S5). Having
422 previously shown that the *pdr6*Δ mutant has no defect in capsule induction, we hypothesized
423 that alterations in the capsular architecture could explain the visually increased exposed
424 cryptococcal PAMPs. To assess this, we used several anti-polysaccharide capsule antibodies to
425 stain the capsules of H99, *pdr6Δ*, and *cap59*Δ cells (Fig. 11F). A significant increase in staining
426 and penetration of the antibody was observed in the *pdr6*Δ mutant when using the mAb 302

427 (Fig. 11F). This antibody only recognizes and binds acetylated GXM (41) and suggests that the
428 integrity and/or porousness of the polysaccharide capsule in the *pdr6*Δ strain is altered when
429 compared to the structurally-sound H99 capsule. This could justify the high-uptake phenotype
430 of the *pdr6*Δ mutant (13, 42). Lastly, we tested if the *pdr6*Δ mutant could form titan cells using
431 a recent *in vitro* induction protocol (43), as titan cells are restricted to the lungs, have an
432 altered cell surface, and are related to latency. Although there was a trend to form less titan
433 cells, it was not statistically significant relative to H99 (Fig. 11G). Altogether, these findings
434 suggest that the deletion of *PDR6* disrupts the cryptococcal cell wall composition and the
435 capsule density (since it is induced to normal size in the *pdr6*Δ mutant), increasing the potential
436 exposure of fungal PAMPs, which can drive the strong pro-inflammatory response by the host
437 immune system.
438

439 **DISCUSSION**

440 Fungal PDR transporters have been primarily studied for their role in antifungal
441 resistance. For example, the overexpression of *AFR1* in *C. neoformans* and *CDR1* in *C. albicans*
442 clinical strains increase their resistance to many of the azole class antifungals and complicates
443 their treatment strategy (44, 45). Structurally, these two proteins (and all other well-
444 characterized fungal PDR transporters) are 'full-length' consisting of two nucleotide-binding
445 domains (NBDs) and two transmembrane domains (TMDs), which is required for a functional
446 fungal PDR protein (15, 16, 46). Here, we continue the characterization of *C. neoformans PDR6*,
447 an atypical and novel 'half-size' PDR transporter since it only possesses one NBD and one TMD.
448 Despite this, various lines of evidence suggest it forms a functional transporter (13, 14).

449 However, we found that in addition to azole resistance, *PDR6* modulates the host immune
450 response, a phenotype that may be unique to 'half-size' PDR transporters (13).

451 The *pdr6*Δ-dependent alterations in survival, fungal burden, and symptoms all suggested
452 a differential host response. Moreover, the fact that despite the significant decrease in fungal
453 burden across organs, and the use of a lower inoculum, the mice still died, suggesting that the
454 *pdr6*Δ-infected mice were not succumbing to uncontrolled fungal growth, but rather to an
455 inappropriate and damaging immune response. This was further supported by the FLC and
456 dexamethasone studies. Treatment of the *pdr6*Δ-infected mice with FLC decreased the fungal
457 burden in all organs, and in some to the limit of detection, and yet the mice still died. In
458 contrast, but consistent with the immune response as the culprit, dexamethasone treatment in
459 the *pdr6*Δ-infected mice significantly extended their survival despite having fungal burdens that
460 were higher than the WT-infected mice at TOD. Lastly, the divergence in symptoms, histological
461 analysis, immune cell quantification, and cytokine/chemokine expression profiles, all were
462 consistent with an aggressive lung pro-inflammatory immune response against the *pdr6*Δ
463 mutant, resulting in their death by pneumonia rather than by CME. We recognize, however,
464 that the *pdr6*Δ-infected mice still had CFUs in the brain, so CME cannot be ruled out, but we
465 believe that it was below the threshold to trigger the neurological symptoms characteristic of
466 CME. This is supported by the "muted" immune response in the brain tissue, indicative of little
467 inflammation, and by the fact that when treated with FLC, there was minimal extrapulmonary
468 dissemination but no change in the outcome of the infection. If we consider that the *pdr6*Δ
469 mutant grows slower under host-like conditions (13), is recognized more avidly by THP-1 cells
470 (alveolar macrophages)(13, 42), and has reduced intracellular survival (13, 14), then the

471 massive lung tissue damage seen in the *pdr6*Δ-infected mice at TOD has to be due to an
472 inappropriate, dysregulated, Th1 immune response.

473 Although treatment with a corticosteroid supported our hypothesis, we acknowledge
474 there are some limitations. Dexamethasone is a strong immunosuppressant, dampening the
475 immune response in the whole body, especially given the length of the study. To address that,
476 we purposefully used doses that corresponded to less than those used in human clinical trials
477 (29). This extended treatment might explain why, even in the combo treatment with FLC, which
478 reduced both inflammation and fungal burden in the lungs and restored tissue architecture
479 almost to normal, the mice appeared so sickly. Optimizing the timing of the dexamethasone
480 treatments, or employing ways to target the drug specifically to the lungs, as with the use of an
481 inhaler, might results in improved outcomes and represents a future direction of investigation.
482 However, we reasoned that we could counter the pro-inflammatory response induced by the
483 *pdr6*Δ mutant using mouse breeds that naturally mount anti-inflammatory, or Th2-skewed,
484 responses to infection, such as the BALB/c mouse. As a control, we also infected C57BL/6 mice,
485 which are known to be Th1-skewed in their immune responses. Again, consistent with our
486 hypothesis, 70% of the BALB/c mice survived until the experimental endpoint at 60 dpi despite
487 having significantly higher lung fungal burdens at this timepoint compared to the H99-infected
488 mice at TOD.

489 The *in vivo* experimentation allowed us to comprehend what was occurring within the
490 host, but why was this specifically occurring with the *pdr6*Δ strain? Our data showing that the
491 *pdr6*Δ mutant displays altered PAMP exposure is a reasonable explanation for the pro-
492 inflammatory response. However, it may not be the only reason as the acapsular *cap59*Δ

493 mutant also exhibits increased PAMP exposure and it is avirulent in the same mouse model.
494 Furthermore, we previously showed that conditioned media (CM) from *pdr6*Δ cultures
495 modulates the phagocytosis of *C. neoformans* by macrophages, whereas the CM from *cap59*Δ
496 or other PDR transporter mutants had little to no effect (13), suggestive of an
497 immunomodulatory Pdr6-dependent secreted factor. Furthermore, other cryptococcal mutants
498 with altered PAMP exposure have been reported but none of them induce an immune response
499 as that seen here with the *pdr6*Δ mutant (47-50). The *mar1*Δ mutant has a disorganized cell
500 wall with increased chitin exposure, less glucans and mannans, and little capsule (49). Like our
501 case, the *mar1*Δ mutant causes a protracted death in C57BL/6 but shows no mortality in BALB/c
502 (47). However, in the *mar1*Δ-infected BALB/c mice, the immune response was controlled in the
503 form of GM-CSF-dependent granulomas and there was no overt pro-inflammatory response,
504 which is different from *pdr6*Δ-infected mice. The *pdr6*Δ-induced mortality is more similar to
505 that seen with the *usv101*Δ strain, which causes fatal pneumonia in A/J mice with little to no
506 extrapulmonary dissemination (50). However, pathologically, the *usv101*Δ mutant did not
507 generate granulomas like the *pdr6*Δ mutant, and in our case, we see much more
508 extrapulmonary dissemination than that with the *usv101*Δ mutant. The *usv101*Δ strain has a
509 larger capsule than WT, thus it might not be exposing the same antigens as the *pdr6*Δ (which
510 has a normal-sized capsule), generating a muted immune response relative to the response
511 induced by *pdr6*Δ. Lastly, the *rim101*Δ mutant also induces a strong pro-inflammatory response
512 in A/J mice as a result of an altered cell surface, but unlike the *pdr6*Δ mutant, it results in
513 hypervirulence rather than a protracted death. Furthermore, the *rim101*Δ-induced immune
514 response is mediated by neutrophils and eosinophils, hence, does not involve granulomas like

515 in the *mar1*Δ or *pdr6*Δ cases. Therefore, an altered exposure of PAMPs alone cannot explain the
516 *pdr6*Δ modulation of the immune response. Consistently, there are examples of cryptococcal
517 mutants that induce altered immune responses without any detectable surface changes, like
518 the F-box protein mutant *fbp1*Δ (48). Overall, this work and the examples discussed indicate
519 that a granulomatous inflammatory response is protective against *Cryptococcus* lung infection.
520 Interestingly, early clinical studies in cryptococcosis patients showed that T cells are needed for
521 an effective containment of fungal cells in a granuloma (51). This is consistent with our finding
522 that at 14 dpi, when the mice are controlling the *pdr6*Δ infection, there is a considerably
523 increase in lymphocytes relative to the WT-infection, while there are no significant changes in
524 innate cells. However, at 35 dpi, percentage-wise, there are almost no lymphocytes in the
525 *pdr6*Δ-infected lungs while there is a significant increase in macrophages (Fig. 11H). Although
526 further studies depleting these cell populations are needed to confirm this, it is conceivable
527 that a failed sustained lymphocyte response is responsible for the eventual death in the *pdr6*Δ-
528 infected mice. Curiously, a recent study from the Nielsen lab found an association between
529 hypervirulence and increased Th1/Th17 immune responses specific to the A/J mouse breed
530 (52). However, in that study, the hypervirulent strains induced a neutrophil-based response
531 while the strong inflammatory response induced by *pdr6*Δ seems to be mediated by
532 macrophages and not by neutrophils (Fig. 11H).

533 Taken together, these data provide important insights for improving the management of
534 CME. Anticryptococcal treatments are limited by toxicity, costs, and rising microbial resistance,
535 but FLC, despite being sub-optimal, still is the antifungal of choice in many regions of the world
536 because it is cheap, relatively less toxic, and broad spectrum. Since the deletion of *PDR6* results

537 in hypersensitivity to FLC, the design and synthesis of a novel compound that targets Pdr6,
538 coupled with FLC and/or a corticosteroid, may have clinical potential. Alternatively, several
539 groups in the cryptococcal and immunology fields have tried to identify potential vaccine
540 candidates against this fungus (53). Collectively, these preliminary vaccines, elicit a pro-
541 inflammatory response allowing for protection against subsequent challenges (54-56).
542 However, this is hampered because the immune mechanisms that elicit a protective immune
543 response are not known yet. Thus, the knowledge generated in this study has potential to help
544 inform cryptococcal vaccine development by providing novel insights into what constitutes a
545 deleterious pro-inflammatory response against *C. neoformans* infection.

546 Finally, the full complexities of PDR half-size transporters remain unknown. It is
547 understood that these proteins are promiscuous and transport a diverse array of substrates,
548 and with the expanded repertoire of PDR genes in *Cryptococcus*, it is not surprising to find roles
549 other than traditional efflux pumps and subsequent resistance to xenobiotics. *PDR6* has also
550 been implicated in aging and replicative life span (14), and most recently, *PDR9*, a full-length
551 PDR gene in the same clade as *AFR1*, was found to play a role in CO_2 tolerance via an unknown
552 mechanism that may involve phospholipid flipping (57). Hence, *PDR6* may act through multiple
553 direct and indirect mechanisms to modulate the inflammatory host response, such as by
554 secreting immunomodulatory molecules, aiding in maintaining the correct PM fluidity by
555 regulating ergosterol transport, and preventing exposure of surface PAMPs by supporting
556 correct cell wall and/or capsule architecture. All of these functions could be mediated by Pdr6-
557 dependent metabolites, lipids, or proteins, supporting future studies in these areas such as
558 comparative metabolomics of WT and *pdr6*Δ CM.

559 In conclusion, we have further characterized a novel PDR transporter in *C. neoformans*
560 by studying the role of *PDR6* in a mouse model of cryptococcosis and examining the altered
561 immune response. Mice infected with the *pdr6*Δ strain develop an overexuberant inflammatory
562 response that is effective at controlling the infection in the lungs short-term, but eventually
563 causes a fulminant pneumonia. Elucidating the role of *PDR6* in the context of infection
564 improves our understanding of cryptococcal pathogenesis while also informing potential
565 clinically-relevant therapeutic studies such as the search for novel drug targets or the
566 development of a vaccine. More broadly, this study expands the field of fungal PDR
567 transporters and given the conserved nature of these proteins, these findings may be
568 applicable to other fungal pathogens.
569

570 **MATERIALS & METHODS**

571 **Strains, media, and growth conditions.**

572 All *C. neoformans* strains used in this study were in the serotype A H99α background. All fungal
573 strains were maintained at -80ºC and grown at 30ºC on yeast peptone dextrose (YPD) with
574 antibiotics (NAT or G418) as appropriate. The *pdr6*Δ strain used for most of these studies was
575 obtained from the Madhani deletion collection (58) and the recreated strains were made in this
576 background by biolistics (13). The genome of all four independently created *pdr6*Δ mutants was
577 sequenced to confirm proper deletion of the gene without additional gross changes.
578 The human monocyte cell line THP-1 (ATCC TIB-202) was grown in THP-1 complete medium and
579 differentiated with phorbol 12-myristate 12-acetate (PMA, Sigma) as described (13). The hAELVi

580 cell line is an immortalized normal human alveolar epithelial cell obtained commercially
581 (InSCREENeX GmbH, Germany) and was grown and used as described (59).

582 **Murine survival studies**

583 *In vivo* fungal virulence was tested using the murine inhalation model of cryptococcosis (13, 42,
584 50, 60). Briefly, 5- to 6-week-old female inbred mice (A/J, C57BL/6, or BALB/c, all from The
585 Jackson Laboratories) were anesthetized with a ketamine rodent cocktail delivered i.p. and
586 intranasally inoculated, unless otherwise stated, with 5.0 x 10^4 cryptococcal cells in 40 µL of
587 sterile PBS. Animals were closely monitored and humanely euthanized if they lost >20% weight
588 relative to peak weight, or at predetermined timepoints, or at the end of the experiment
589 (maximum of 60 days). For drug treatment studies, cryptococcal-infected mice were randomly
590 assigned into treated or non-treated control groups. Stock solutions of fluconazole (1.6 mg/mL),
591 dexamethasone (0.03 mg/mL), and a fluconazole/dexamethasone combo were prepared in
592 sterile PBS. The drug(s) were administered intraperitoneally at doses of 16 mg/kg/day or 8
593 mg/kg/day for fluconazole, and of 0.3 mg/kg/day for dexamethasone. Treatment with these
594 compounds began 24 h after infection and continued throughout the experiment until endpoint
595 was reached. Statistically significant differences between survival curves were determined by
596 log rank Mantel-Cox test (GraphPad Prism). All of the mouse infections and procedures were
597 approved by the University of Notre Dame Institutional Animal Care and Use Committee
598 (protocol #23-05-7918).

599 **Fungal Burden Quantification**

600 Infected mice were humanely euthanized at predetermined time points or TOD by isoflurane
601 overdose followed by cervical dislocation, and lungs, brain, and spleens were harvested. Tissues

602 were homogenized in 5 mL of sterile PBS, diluted, and plated on YPD agar medium
603 supplemented with ampicillin. CFUs were counted following incubation at 30ºC for 48 h.
604 Statistical significance was determined using ANOVA Kruskal-Wallis test (GraphPad Prism).

605 **Histological analyses**

606 A/J female mice (The Jackson Laboratories) were infected via the intranasal route as described
607 above with 5 x 10^4 CFU of either WT (H99) or the *pdr6*Δ mutant strain. Mice were sacrificed as
608 predetermined time points (14, 35, 50 days post inoculation) by isoflurane overdose followed
609 by cervical dislocation. Lungs were perfused with sterile PBS and 10% neutralized formalin.
610 Lungs were subsequently paraffin embedded, sectioned, mounted, and stained with H&E by the
611 University of Notre Dame Histology Core facility. H&E-stained slides were imaged at 10X and
612 40X using an inverted Zeiss microscope. Slides were scored in a blind manner by the resident
613 pathologist at the Harper Cancer Research Institute.

614 **Cytokine Analyses**

615 Female mice (A/J, C57BL/6, or BALB/c, all from The Jackson Labs) were infected via the
616 intranasal route with WT (H99) or the *pdr6*Δ mutant strain as described above. Mice were
617 euthanized at predetermined time points by isoflurane overdose followed by cervical
618 dislocation. Cytokine levels within the A/J mice lung and brain homogenates were analyzed
619 using the Proteome Profiler Mouse XL Cytokine Array (R&D Systems Inc., Minneapolis, MN). The
620 relative expression levels of 111 soluble mouse proteins were determined following the
621 manufacturer's protocol. Array membranes were imaged using LI-COR Odyssey Infrared
622 Imaging System and quantified using ImageStudio software. Cytokine/chemokine expression
623 levels were further confirmed in A/J mice, as well as in C57BL/6 and BALB/c mice, using the Bio-

624 Plex Multi-Plex Assay Kit (Bio-Rad Laboratories, Hercules, CA). Supernatants from organ
625 homogenates were used to determine presence of 22 proteins including eotaxin, G-CSF, GM-
626 CSF, IFN-γ, IL-1α, IL-1β, IL-2, IL-3, IL-4, IL-6, IL-9, IL-10, IL-12 (p40), IL-12 (p70), IL-13, IL-17A, KC,
627 MCP-1, MCP-1α, MIP-1β, RANTES, and TNF-α.

628 **Pulmonary leukocyte isolation and flow cytometric analysis**

629 H99 and *pdr6*Δ-infected A/J mice were euthanized at predetermined time points and TOD by
630 isoflurane overdose followed by cervical dislocation. Lungs of infected mice were excised and
631 digested enzymatically at 37ºC for 60 min in 10 mL of digest buffer (0.34 U/mL Liberase™
632 (Roche) and 100 ug/mL DNaseI (ThermoFisher)) in 1X DPBS. After 60 min, digestion was
633 arrested with 1X DPBS supplemented with 2% FBS and 0.2 um EDTA. The cell suspension was
634 washed and passed through 40-μm cell strainers. The single cell suspensions were stained with
635 a live/dead far red viability dye (Invitrogen), washed, and incubated on ice for 20 min with
636 purified anti-mouse CD16/CD32 antibodies (BioLegend) to block Fc receptors. Following
637 blocking, cells were incubated with fluorochrome-conjugated antibodies to allow for
638 multistaining for 45 min on ice. The innate panel consisted of PE-Cy5 conjugated anti-CD45 (30-
639 111), Brilliant Violet (BV) 650-conjugated anti-CD11b (M1/70), Super Bright (SB) 780-conjugated
640 anti-F4/80 (BM8), BV711-conjugated anti-Ly6G (1A8), PE-Cy7-conjugated anti-Ly6C (HK1.4), PE-
641 conjugated anti-SiglecF (1RNM44N), and APC-eFluor 780-conjugated anti-CD11c (N418). The
642 adaptive panel included PE-Cy5 conjugated anti-CD45 (30-111), AF700-conjugated anti-CD3
643 (145-2C11), BV421-conjugated anti-CD4 (GK1.5), BV510-conjugated anti-CD25 (PC61-5), PE-
644 conjugated anti-CD8 (53-6.7), and AF488-conjugated anti-FoxP3 (FJK-16s). Cells were washed
645 and fixed with 2% formalin in FACS buffer. UltraComp eBeads (Invitrogen) were stained with

646 each respective fluorochrome-conjugated antibody and used to determine and
647 spillover/compensation calculations. Data was analyzed using FlowJo software.

648 **Cell wall and capsule stains**

649 Starter cultures were grown overnight in YPD, washed with DMEM, and 1 x 10^6 cells/mL were
650 added to 24-well tissue culture plates. Plates were incubated at 37ºC + 5% CO2 for 48 h. The
651 cells were collected by centrifugation at 3,000 x g for 5 min. For staining, Calcofluor White
652 (CFW), Alexa Fluor 488-conjugated concanavalin A (ConA), β-(1,3)-glucan antibody 2GB
653 (ab233743; Abcam, USA), eosin Y (EoY), and the capsular antibody 302 were used. Cells were
654 washed and stained with CFW, ConA, β-(1,3)-glucan antibody, EoY, and Mab 302 at 100 µg/mL,
655 50 µg/mL, 20 µg/mL, 500 µg/mL, and 10 µg/mL, respectively. Cells were incubated with the
656 stains for 30 min, washed, fixed, and imaged at 100X using an inverted Zeiss microscope.
657 Fluorescence of mAb 302 was calculated using Cell Profiler software. Flow cytometry data was
658 acquired using a BD LSRFortessa cytometer. The CFW signal was detected using a 405 nm laser
659 and the ConA and EoY signals were detected using a 488 nm laser. Flow cytometry data was
660 analyzed with FlowJo software.

661

662 **ACKNOWLEDGMENTS**

663 We acknowledge assistance and support on the murine studies from the University of Notre
664 Dame Freimann Life Science Center (FLSC). We give a special thanks to William J. Kaliney, M.D.,
665 pathologist from Harper Cancer Research Center, for assistance with histological analysis and
666 scoring. We acknowledge financial support from the Warren Center for Drug Discovery (pilot
667 grant) and NIH grant R21AI71742. Other related work in the Santiago-Tirado lab is supported by

668 NIH grant R01AI177875. We also thank members of the Santiago-Tirado lab for their thoughtful
669 comments and feedback on this work.

670

671 **REFERENCES**

672 1. Denning DW. 2024. Global incidence and mortality of severe fungal disease. Lancet Infect Dis
673 doi:10.1016/S1473-3099(23)00692-8.
674 2. Gaylord EA, Choy HL, Doering TL. 2020. Dangerous Liaisons: Interactions of Cryptococcus
675 neoformans with Host Phagocytes. Pathogens 9.
676 3. Stuckey PV, Santiago-Tirado FH. 2023. Fungal mechanisms of intracellular survival: what can we
677 learn from bacterial pathogens? Infect Immun 91:e0043422.
678 4. Rajasingham R, Govender NP, Jordan A, Loyse A, Shroufi A, Denning DW, Meya DB, Chiller TM,
679 Boulware DR. 2022. The global burden of HIV-associated cryptococcal infection in adults in
680 2020: a modelling analysis. Lancet Infect Dis doi:10.1016/S1473-3099(22)00499-6.
681 5. Santiago-Tirado FH, Doering TL. 2017. False friends: Phagocytes as Trojan horses in microbial
682 brain infections. PLoS Pathog 13:e1006680.
683 6. Denham ST, Brown JCS. 2018. Mechanisms of Pulmonary Escape and Dissemination by
684 Cryptococcus neoformans. J Fungi (Basel) 4.
685 7. Zaragoza O, Rodrigues ML, De Jesus M, Frases S, Dadachova E, Casadevall A. 2009. The capsule
686 of the fungal pathogen Cryptococcus neoformans. Adv Appl Microbiol 68:133-216.
687 8. Denham ST, Verma S, Reynolds RC, Worne CL, Daugherty JM, Lane TE, Brown JCS. 2018.
688 Regulated Release of Cryptococcal Polysaccharide Drives Virulence and Suppresses Immune Cell
689 Infiltration into the Central Nervous System. Infect Immun 86.
690 9. Eisenman HC, Casadevall A. 2012. Synthesis and assembly of fungal melanin. Appl Microbiol
691 Biotechnol 93:931-40.
692 10. Alspaugh JA. 2015. Virulence mechanisms and Cryptococcus neoformans pathogenesis. Fungal
693 Genet Biol 78:55-8.
694 11. Pacelli C, Bryan RA, Onofri S, Selbmann L, Shuryak I, Dadachova E. 2017. Melanin is effective in
695 protecting fast and slow growing fungi from various types of ionizing radiation. Environ
696 Microbiol 19:1612-1624.
697 12. Ueno K, Nagamori A, Honkyu NO, Kataoka M, Shimizu K, Chang YC, Kwon-Chung KJ, Miyazaki Y.
698 2023. Cryptococcus neoformans requires the TVF1 gene for thermotolerance and virulence.
699 Med Mycol 61.
700 13. Winski CJ, Qian Y, Mobashery S, Santiago-Tirado FH. 2022. An Atypical ABC Transporter Is
701 Involved in Antifungal Resistance and Host Interactions in the Pathogenic Fungus *Cryptococcus*
702 *neoformans*. mBio 13:e0153922.
703 14. Oliveira NK, Bhattacharya S, Gambhir R, Joshi M, Fries BC. 2022. Novel ABC Transporter
704 Associated with Fluconazole Resistance in Aging of Cryptococcus neoformans. J Fungi (Basel) 8.
705 15. Moreno A, Banerjee A, Prasad R, Falson P. 2019. PDR-like ABC systems in pathogenic fungi. Res
706 Microbiol 170:417-425.
707 16. Khunweeraphong N, Kuchler K. 2021. Multidrug Resistance in Mammals and Fungi-From MDR to
708 PDR: A Rocky Road from Atomic Structures to Transport Mechanisms. Int J Mol Sci 22.
709 17. Jankovic D, Liu Z, Gause WC. 2001. Th1- and Th2-cell commitment during infectious disease:
710 asymmetry in divergent pathways. Trends Immunol 22:450-7.

711 18. Stacey AR, Norris PJ, Qin L, Haygreen EA, Taylor E, Heitman J, Lebedeva M, DeCamp A, Li D,
712 Grove D, Self SG, Borrow P. 2009. Induction of a striking systemic cytokine cascade prior to peak
713 viremia in acute human immunodeficiency virus type 1 infection, in contrast to more modest
714 and delayed responses in acute hepatitis B and C virus infections. J Virol 83:3719-33.
715 19. McMichael AJ, Borrow P, Tomaras GD, Goonetilleke N, Haynes BF. 2010. The immune response
716 during acute HIV-1 infection: clues for vaccine development. Nat Rev Immunol 10:11-23.
717 20. Wozniak KL, Ravi S, Macias S, Young ML, Olszewski MA, Steele C, Wormley FL. 2009. Insights into
718 the mechanisms of protective immunity against Cryptococcus neoformans infection using a
719 mouse model of pulmonary cryptococcosis. PLoS One 4:e6854.
720 21. Wozniak KL, Hardison S, Olszewski M, Wormley FL, Jr. 2012. Induction of protective immunity
721 against cryptococcosis. Mycopathologia 173:387-94.
722 22. Chang CC, Harrison TS, Bicanic TA, Chayakulkeeree M, Sorrell TC, Warris A, Hagen F, Spec A,
723 Oladele R, Govender NP, Chen SC, Mody CH, Groll AH, Chen YC, Lionakis MS, Alanio A, Castaneda
724 E, Lizarazo J, Vidal JE, Takazono T, Hoenigl M, Alffenaar JW, Gangneux JP, Soman R, Zhu LP,
725 Bonifaz A, Jarvis JN, Day JN, Klimko N, Salmanton-Garcia J, Jouvion G, Meya DB, Lawrence D,
726 Rahn S, Bongomin F, McMullan BJ, Sprute R, Nyazika TK, Beardsley J, Carlesse F, Heath CH,
727 Ayanlowo OO, Mashedi OM, Queiroz-Telles Filho F, Hosseinipour MC, Patel AK, Temfack E, Singh
728 N, Cornely OA, Boulware DR, et al. 2024. Global guideline for the diagnosis and management of
729 cryptococcosis: an initiative of the ECMM and ISHAM in cooperation with the ASM. Lancet Infect
730 Dis doi:10.1016/S1473-3099(23)00731-4.
731 23. Rothe C, Sloan DJ, Goodson P, Chikafa J, Mukaka M, Denis B, Harrison T, van Oosterhout JJ,
732 Heyderman RS, Lalloo DG, Allain T, Feasey NA. 2013. A prospective longitudinal study of the
733 clinical outcomes from cryptococcal meningitis following treatment induction with 800 mg oral
734 fluconazole in Blantyre, Malawi. PLoS One 8:e67311.
735 24. Coelho C, Casadevall A. 2016. Cryptococcal therapies and drug targets: the old, the new and the
736 promising. Cell Microbiol 18:792-9.
737 25. Zhang J, Li L, Lv Q, Yan L, Wang Y, Jiang Y. 2019. The Fungal CYP51s: Their Functions, Structures,
738 Related Drug Resistance, and Inhibitors. Front Microbiol 10:691.
739 26. Casadevall A. 2022. Immunity to Invasive Fungal Diseases. Annu Rev Immunol 40:121-141.
740 27. Qiu Y, Dayrit JK, Davis MJ, Carolan JF, Osterholzer JJ, Curtis JL, Olszewski MA. 2013. Scavenger
741 receptor A modulates the immune response to pulmonary Cryptococcus neoformans infection. J
742 Immunol 191:238-48.
743 28. Brinks J, van Dijk EHC, Habeeb M, Nikolaou A, Tsonaka R, Peters HAB, Sips HCM, van de Merbel
744 AF, de Jong EK, Notenboom RGE, Kielbasa SM, van der Maarel SM, Quax PHA, Meijer OC, Boon
745 CJF. 2018. The Effect of Corticosteroids on Human Choroidal Endothelial Cells: A Model to Study
746 Central Serous Chorioretinopathy. Invest Ophthalmol Vis Sci 59:5682-5692.
747 29. Day J, Imran D, Ganiem AR, Tjahjani N, Wahyuningsih R, Adawiyah R, Dance D, Mayxay M,
748 Newton P, Phetsouvanh R, Rattanavong S, Chan AK, Heyderman R, van Oosterhout JJ, Chierakul
749 W, Day N, Kamali A, Kibengo F, Ruzagira E, Gray A, Lalloo DG, Beardsley J, Binh TQ, Chau TT,
750 Chau NV, Cuc NT, Farrar J, Hien TT, Van Kinh N, Merson L, Phuong L, Tho LT, Thuy PT, Thwaites
751 G, Wertheim H, Wolbers M. 2014. CryptoDex: a randomised, double-blind, placebo-controlled
752 phase III trial of adjunctive dexamethasone in HIV-infected adults with cryptococcal meningitis:
753 study protocol for a randomised control trial. Trials 15:441.
754 30. Kitonsa J, Nsubuga R, Mayanja Y, Kiwanuka J, Nikweri Y, Onyango M, Anywaine Z, Ggayi AB,
755 Kibengo FM, Kaleebu P, Day J. 2020. Determinants of two-year mortality among HIV positive
756 patients with Cryptococcal meningitis initiating standard antifungal treatment with or without
757 adjunctive dexamethasone in Uganda. PLoS Negl Trop Dis 14:e0008823.

758 31. Netea MG, Schlitzer A, Placek K, Joosten LAB, Schultze JL. 2019. Innate and Adaptive Immune
759 Memory: an Evolutionary Continuum in the Host's Response to Pathogens. Cell Host Microbe
760 25:13-26.
761 32. Rudman J, Evans RJ, Johnston SA. 2019. Are macrophages the heroes or villains during
762 cryptococcosis? Fungal Genet Biol 132:103261.
763 33. Hole C, Wormley FL, Jr. 2016. Innate host defenses against Cryptococcus neoformans. J
764 Microbiol 54:202-11.
765 34. Hole CR, Lam WC, Upadhya R, Lodge JK. 2020. Cryptococcus neoformans Chitin Synthase 3 Plays
766 a Critical Role in Dampening Host Inflammatory Responses. mBio 11.
767 35. O'Halloran JA, Powderly WG, Spec A. 2017. Cryptococcosis today: It is not all about HIV
768 infection. Curr Clin Microbiol Rep 4:88-95.
769 36. Koselny K, Mutlu N, Minard AY, Kumar A, Krysan DJ, Wellington M. 2018. A Genome-Wide
770 Screen of Deletion Mutants in the Filamentous Saccharomyces cerevisiae Background Identifies
771 Ergosterol as a Direct Trigger of Macrophage Pyroptosis. mBio 9.
772 37. Rodrigues ML. 2018. The Multifunctional Fungal Ergosterol. mBio 9.
773 38. Pasrija R, Panwar SL, Prasad R. 2008. Multidrug transporters CaCdr1p and CaMdr1p of Candida
774 albicans display different lipid specificities: both ergosterol and sphingolipids are essential for
775 targeting of CaCdr1p to membrane rafts. Antimicrob Agents Chemother 52:694-704.
776 39. Xu X, Bittman R, Duportail G, Heissler D, Vilcheze C, London E. 2001. Effect of the structure of
777 natural sterols and sphingolipids on the formation of ordered sphingolipid/sterol domains
778 (rafts). Comparison of cholesterol to plant, fungal, and disease-associated sterols and
779 comparison of sphingomyelin, cerebrosides, and ceramide. J Biol Chem 276:33540-6.
780 40. Upadhya R, Lam WC, Hole CR, Vasselli JG, Lodge JK. 2023. Cell wall composition in Cryptococcus
781 neoformans is media dependent and alters host response, inducing protective immunity. Front
782 Fungal Biol 4.
783 41. Kozel TR, Levitz SM, Dromer F, Gates MA, Thorkildson P, Janbon G. 2003. Antigenic and
784 biological characteristics of mutant strains of Cryptococcus neoformans lacking capsular O
785 acetylation or xylosyl side chains. Infect Immun 71:2868-75.
786 42. Santiago-Tirado FH, Peng T, Yang M, Hang HC, Doering TL. 2015. A Single Protein S-acyl
787 Transferase Acts through Diverse Substrates to Determine Cryptococcal Morphology, Stress
788 Tolerance, and Pathogenic Outcome. PLoS Pathog 11:e1004908.
789 43. Dambuza IM, Drake T, Chapuis A, Zhou X, Correia J, Taylor-Smith L, LeGrave N, Rasmussen T,
790 Fisher MC, Bicanic T, Harrison TS, Jaspars M, May RC, Brown GD, Yuecel R, MacCallum DM,
791 Ballou ER. 2018. The Cryptococcus neoformans Titan cell is an inducible and regulated
792 morphotype underlying pathogenesis. PLoS Pathog 14:e1006978.
793 44. Posteraro B, Sanguinetti M, Sanglard D, La Sorda M, Boccia S, Romano L, Morace G, Fadda G.
794 2003. Identification and characterization of a Cryptococcus neoformans ATP binding cassette
795 (ABC) transporter-encoding gene, CnAFR1, involved in the resistance to fluconazole. Mol
796 Microbiol 47:357-71.
797 45. Prasad R, De Wergifosse P, Goffeau A, Balzi E. 1995. Molecular cloning and characterization of a
798 novel gene of Candida albicans, CDR1, conferring multiple resistance to drugs and antifungals.
799 Curr Genet 27:320-9.
800 46. Lamping E, Baret PV, Holmes AR, Monk BC, Goffeau A, Cannon RD. 2010. Fungal PDR
801 transporters: Phylogeny, topology, motifs and function. Fungal Genet Biol 47:127-42.
802 47. Telzrow CL, Esher Righi S, Castro-Lopez N, Campuzano A, Brooks JT, Carney JM, Wormley FL, Jr.,
803 Alspaugh JA. 2022. An Immunogenic and Slow-Growing Cryptococcal Strain Induces a Chronic
804 Granulomatous Infection in Murine Lungs. Infect Immun 90:e0058021.

805 48. Masso-Silva J, Espinosa V, Liu TB, Wang Y, Xue C, Rivera A. 2018. The F-Box Protein Fbp1 Shapes
806 the Immunogenic Potential of Cryptococcus neoformans. mBio 9.
807 49. Esher SK, Ost KS, Kohlbrenner MA, Pianalto KM, Telzrow CL, Campuzano A, Nichols CB, Munro C,
808 Wormley FL, Jr., Alspaugh JA. 2018. Defects in intracellular trafficking of fungal cell wall
809 synthases lead to aberrant host immune recognition. PLoS Pathog 14:e1007126.
810 50. Gish SR, Maier EJ, Haynes BC, Santiago-Tirado FH, Srikanta DL, Ma CZ, Li LX, Williams M, Crouch
811 EC, Khader SA, Brent MR, Doering TL. 2016. Computational Analysis Reveals a Key Regulator of
812 Cryptococcal Virulence and Determinant of Host Response. MBio 7:e00313-16.
813 51. Hill JO. 1992. CD4+ T cells cause multinucleated giant cells to form around Cryptococcus
814 neoformans and confine the yeast within the primary site of infection in the respiratory tract. J
815 Exp Med 175:1685-95.
816 52. Ding M, Jackson KM, Harris-Gordon M, Dileepan T, Meya DB, Nielsen K. 2025. The hypervirulent
817 Type-1/Type-17 phenotype of Cryptococcus neoformans clinical isolates is specific to A/J mice.
818 Infect Immun 93:e0058524.
819 53. Del Poeta M, Wormley FL, Jr., Lin X. 2023. Host populations, challenges, and commercialization
820 of cryptococcal vaccines. PLoS Pathog 19:e1011115.
821 54. Wang Y, Wang K, Rivera A, Xue C. 2023. Development of a Heat-Killed fbp1 Mutant Strain as a
822 Therapeutic Agent To Treat Invasive Cryptococcus Infection. Microbiol Spectr 11:e0495522.
823 55. Pham T, Li Y, Watford W, Lin X. 2023. Vaccination with a ZNF2(oe) Strain of Cryptococcus
824 Provides Long-Lasting Protection against Cryptococcosis and Is Effective in
825 Immunocompromised Hosts. Infect Immun 91:e0019823.
826 56. Wormley FL, Jr., Perfect JR, Steele C, Cox GM. 2007. Protection against cryptococcosis by using a
827 murine gamma interferon-producing *Cryptococcus neoformans* strain. Infect Immun 75:1453-62.
828 57. Ristow LC, Jezewski AJ, Chadwick BJ, Stamnes MA, Lin X, Krysan DJ. 2023. Cryptococcus
829 neoformans adapts to the host environment through TOR-mediated remodeling of phospholipid
830 asymmetry. Nat Commun 14:6587.
831 58. Liu OW, Chun CD, Chow ED, Chen C, Madhani HD, Noble SM. 2008. Systematic genetic analysis
832 of virulence in the human fungal pathogen *Cryptococcus neoformans*. Cell 135:174-188.
833 59. Kuehn A, Kletting S, de Souza Carvalho-Wodarz C, Repnik U, Griffiths G, Fischer U, Meese E,
834 Huwer H, Wirth D, May T, Schneider-Daum N, Lehr CM. 2016. Human alveolar epithelial cells
835 expressing tight junctions to model the air-blood barrier. ALTEX 33:251-60.
836 60. Santiago-Tirado FH, Hurtaux T, Geddes-McAlister J, Nguyen D, Helms V, Doering TL, Romisch K.
837 2023. The ER Protein Translocation Channel Subunit Sbh1 Controls Virulence of Cryptococcus
838 neoformans. mBio 14:e0338422.

839

840

841

842

843

844 **Figure legends and Table captions**

845 **Fig. 1. *C. neoformans pdr6*Δ-infected mice succumb to infection despite decreased fungal**
846 **burden. (A)** Quantification of fungal burden over time to monitor disease progression. Mice

847 were inoculated with 5 x 10^4 cells and sacrificed every 7 days and organs were harvested to
848 determine CFUs. Significance was determined using Mann-Whitney test, *P<0.05. **(B)** Survival
849 studies of animals infected with H99 and *pdr6*Δ strains, or mock-infected (PBS). 4 A/J mice per
850 group were intranasally infected with 5 x 10^3 cryptococcal cells or mock infected with sterile
851 PBS and monitored for 38 days (experiment was terminated when the last infected mouse
852 reached endpoint). Significance was determined using Mantel-Cox test, **P<0.01. **(C)**
853 Quantified organ burdens of H99 and *pdr6*Δ-infected mice at TOD. Organs were harvested,
854 homogenized, and dilutions were plated on YPD. Plates were incubated for 48 h and CFUs were
855 counted. Each data point represents a mouse and black bars represent the mean. Significance
856 was determined using Mann-Whitney test, *P<0.05; **P<0.01.

857

858 **Fig. 2. Infection with *C. neoformans pdr6*Δ results in altered histopathology. (A & B)** Dissected
859 lungs of female A/J mice infected with 5 x 10^4 cells of the WT strain (H99) or *pdr6*Δ mutant
860 strain, or mock-infected, were harvested at predetermined endpoints of 14 **(A)** and 35 **(B)** dpi.
861 Gross organ examination revealed significant changes in inflammation and tissue damage. H&E
862 staining was used to visualize microscopic lung pathology (inset depicted by the green boxes is
863 shown in the 40X column). The 10X scale bar is 200 μm and the 40X scale bar is 50 μm.

864

865 **Table 1. Quantitative analysis of H99 and *pdr6*Δ-infected lung sections over time.**
866 *All H99-infected mice had succumbed to infection by this timepoint.
867 Histiocytes refer to leukocytes of the monocyte/macrophage/dendritic cell lineage.
868 hpf, high power field.

869

870 **Fig. 3. FLC treatment significantly reduces CFUs in *pdr6*Δ-infected mice without changing the**
871 **outcome. (A)** Survival curve of H99 and *pdr6*Δ-infected mice treated daily with either 8 or 16
872 mg/kg FLC. At least 4 A/J mice per group were intranasally infected with 5 x 10^4 cells, or mock-
873 infected with DPBS and monitored for up to 50 dpi (mock-infected and FLC-treated mice not
874 shown for clarity). Significance was determined using Mantel-Cox test, *P<0.05; **P<0.01;
875 ***P<0.001; ****P<0.0001. **(B-G)** Calculated organ burdens at 14 dpi **(B-D)** or endpoint **(E-G)**.
876 Organs were harvested, homogenized, and dilutions were plated on YPD. Plates were incubated
877 for 48 hr and CFUs were enumerated. Each data point represents a mouse and black bars
878 represent the mean. Significance was determined using one-way ANOVA with multiple
879 comparisons (Welch's corrected), *P<0.05; **P<0.01; ****P<0.0001.

880

881 **Fig. 4. FLC treatment improves lung pathology in *pdr6*Δ-infected animals.** Dissected lungs of
882 female A/J mice infected with 5 x 10^4 cells of the WT strain (H99) or *pdr6*Δ mutant strain and
883 treated daily with 16 mg/kg FLC were harvested at 14 and 35 dpi. Gross organ examination

884 revealed alterations in fungal containment and disease progression. H&E staining was used to
885 visualize microscopic lung pathology. Insets 1 & 2 highlight differential histopathology in the
886 FLC-treated *pdr6*Δ-infected mice at 35 dpi (inset depicted by the green boxes is shown in the
887 40X column). Inset 1 shows an intact lung parenchyma with several fungi and immune cells
888 while inset 2 is characterized as a granuloma. The 10X scale bar is 200 μm and the 40X scale bar
889 is 50 μm.

890

891 **Table 2. Quantitative analysis of Fluconazole treated H99 and *pdr6*Δ-infected lung sections**
892 **over time**
893 Histiocytes refer to leukocytes of the monocyte/macrophage/dendritic cell lineage. hpf, high
894 power field.

895

896 **Fig. 5 Infection with the *pdr6*Δ mutant elicits a robust pro-inflammatory immune response. (A**
897 **& B)** Heatmap of the pro-inflammatory and anti-inflammatory cytokines/chemokines in the
898 lungs **(A)** and brains **(B)** of *C. neoformans*-infected mice. Female A/J mice were intranasally
899 infected with 5 x 10^4 cells of the H99 or *pdr6*Δ strain and euthanized at endpoint. Homogenates
900 from the lungs and brain of at least 4 mice per group were used to perform Proteome Profiler
901 Mouse XL Cytokine Arrays and Bio-Plex Multi-Plex Arrays. **(C & D)** Expression of selected
902 cytokines/chemokines in the lungs **(C)** and brains **(D)** of *pdr6*Δ-infected mice was normalized to
903 H99 (dotted line). Significance was determined by Ordinary 2-way ANOVA with multiple
904 comparisons, *P<0.05; **P<0.01; ***P<0.001; ****P<0.0001.

905

906 **Fig. 6 Dexamethasone treatment significantly extends survival of *pdr6*Δ-infected mice. (A)**
907 Survival curve of H99 and *pdr6*Δ-infected mice treated daily with either 0.03 mg/kg Dexa or
908 0.03 mg/kg Dexa and 16 mg/kg FLC. At least 3 A/J mice per group were intranasally infected
909 with 5 x 10^4 cells, or mock-infected with DPBS and monitored for up to 60 dpi (mock-infected
910 and treated mice not shown for clarity). Significance was determined using Mantel-Cox test,
911 **P<0.01; ****P<0.0001. **(B-G)** Calculated organ burdens at 14 dpi **(B-D)** or endpoint **(E-G)**.
912 Organs were harvested, homogenized, and dilutions were plated on YPD. Plates were incubated
913 for 48 hr and CFUs were enumerated. Each data point represents a mouse and black bars
914 represent the mean. Significance was determined using one-way ANOVA with multiple
915 comparisons (Welch's corrected) *P<0.05; **P<0.01; ***P<0.001.

916

917 **Fig. 7. Effect of dexamethasone treatment on lung histopathology.** Dissected lungs of female
918 A/J mice infected with 5 x 10^4 cells of the WT strain (H99) or *pdr6*Δ mutant strain and treated
919 daily with 0.3 mg/kg Dexa and harvested at 14 and 35 dpi. Gross organ examination revealed

920 alterations in levels of inflammation. H&E staining was used to visualize microscopic lung
921 pathology (inset [green boxes]). The 10X scale bar is 200 μm and the 40X scale bar is 50 μm.

922

923 **Table 3. Quantitative analysis of dexamethasone-treated H99 and *pdr6*Δ-infected lung**
924 **sections over time**
925 Histiocytes refer to leukocytes of the monocyte/macrophage/dendritic cell lineage.
926 hpf, high power field.

927

928 **Fig. 8. Effect of dexamethasone/FLC combination treatment on lung histopathology.**
929 Dissected lungs of female A/J mice infected with 5 x 10^4 cells of the WT strain (H99) or *pdr6*Δ
930 mutant strain and treated daily with a combination of 0.3 mg/kg Dexa and 16 mg/kg FLC and
931 harvested at 14 and 35 dpi. Gross organ examination revealed alterations in levels of
932 inflammation. H&E staining was used to visualize microscopic lung pathology (inset [green
933 boxes]). The 10X scale bar is 200 μm and the 40X scale bar is 50 μm.

934

935 **Table 4. Quantitative analysis of combination Dexamethasone + Fluconazole treated H99 and**
936 ***pdr6*Δ-infected lung sections over time**
937 Histiocytes refer to leukocytes of the monocyte/macrophage/dendritic cell lineage.
938 hpf, high power field.

939

940 **Fig. 9 Infection with the *C. neoformans pdr6Δ* mutant generates an increase in innate immune**
941 **cells, specifically macrophages. (A-H)** Quantification of innate and adaptive immune cell
942 populations at 14 dpi **(A-D)** and endpoint (35 dpi for *pdr6*Δ-infected mice)**(E-H)**. Female A/J
943 mice were intranasally infected with 5 x 10^4 cells of the WT type (H99) or *pdr6*Δ strain and
944 euthanized at clinical endpoints corresponding to imminent mortality. Lungs were harvested
945 and single-cell suspensions were generated and stained with immune panels to quantify
946 monocytes (CD45+F4/80-CD11b+Ly6C+), neutrophils (CD45+F4/80-CD11b+Ly6G+),
947 macrophages (CD45+F4/80+CD11b+), $CD4^+$ Th (CD45+CD3+CD4+), $CD4^+$ T-regs
948 (CD45+CD3+CD4+CD25+FoxP3+), and $CD8^+$ (CD45+CD3+CD8+) cells. Samples were processed
949 using flow cytometry and are presented as total # cells **(A, C, E, G)** or as % $CD45^+$ cells **(B, D, F,**
950 **H)**. Significance was determined using one-way ANOVA with multiple comparisons (Welch's
951 corrected) *P<0.05; **P<0.01. Note: for **G** and **H**, the $CD8^+$ T cell panel could not be run for the
952 day 35 samples, hence they were removed from the H99 bars.

953

954 **Fig. 10 Mice breeds with skewed immune responses influence the outcome of the *pdr6*Δ**
955 **infection.** Survival curves and organ burdens for C57BL/6 **(A – D)** or BALB/c **(F – I)** mice infected

956 with 5 x 10^4 cells of WT (H99) or *pdr6*Δ strains. At least 5 mice were infected for each group.
957 Significance in the survival curves was determined using Mantel-Cox test, **P<0.01;
958 ***P<0.001. For fungal burdens, organs were harvested, homogenized, and dilutions were
959 plated on YPD. Plates were incubated for 48 hr and CFUs were enumerated. Each data point
960 represents a mouse and black bars represent the mean. In panels G-I, crossed data points
961 represent the values from the mice that succumbed to infection. Significance was determined
962 using one-way ANOVA with multiple comparisons (Welch's corrected), *P<0.05. **(E & J)**
963 Heatmap of the pro-inflammatory and anti-inflammatory cytokines/chemokines in the lungs of
964 C57BL/6 **(E)** and BALB/c **(J)** infected mice. Values are shown normalized to age-match mock-
965 infected mice.

966

967 **Fig. 11 *C. neoformans pdr6*Δ cells display altered cell wall features and capsule density. (A)**
968 Visualization of calcofluor (CFW), Alexa488-conjugated Concanavalin A (ConA), and β-(1,3)-
969 glucan staining in H99, *pdr6*Δ-L (from commercial deletion collection), and *cap59*Δ cells.
970 Representative images of stained cells. Scale bar, 10 µm. **(B - E)** Quantification of CFW **(B)**, ConA
971 **(C)**, Eosin Y **(D)**, and β-glucan **(E)** staining intensity in H99, *pdr6*Δ, and *cap59*Δ strains. Staining
972 intensity was measured by flow cytometry and results normalized to H99 (dotted line). Four
973 independent *pdr6*Δ strains were tested (*pdr6*Δ-L and *pdr6*Δ-1 to -3). Significance was
974 determined using one-way ANOVA (Welch's corrected), *P<0.05; ***P<0.001; ****P<0.0001.
975 **(F)** Visualization and quantification of capsular antibody staining of H99, *pdr6*Δ, and *cap59*Δ
976 strains. Cells were stained with anti-capsule mAb 302 and imaged using an inverted Zeiss
977 microscope. Representative images of stained cells. Staining intensity was quantified using a
978 Cell Profiler pipeline. Significance was determined using one-way ANOVA (Welch's corrected)
979 ***P<0.001. **(G)** The % of titanization of the indicated strains was determined as described in
980 the methods. Each data point represents the average % of titanization in independent biological
981 experiments each with at least 100 cells quantified. One-way ANOVA with multiple
982 comparisons, ***P<0.001; ****P<0.0001. **(H)** Model explaining how *pdr6*Δ strains alter disease
983 progression in A/J and C57BL/6 mice, causing fatal pneumonia rather than the typical
984 meningitis caused by H99. The *pdr6*Δ strain has an altered cell surface, including a less dense
985 capsule that is more permeable to antibodies, that results in exposure of pro-inflammatory
986 antigens. This results in an initial immune response that can control the infection, consisting on
987 an increased number of CD4 lymphocytes. However, that initial response is not enough to clear
988 the infection, and eventually results in dysregulation, with a drop in the number of CD4
989 lymphocytes and a dramatic increase in inflammatory macrophages. Despite having less fungal
990 burden in the lungs and little dissemination, the mice succumb to the infection due to too much
991 lung tissue damage. This illustration was originally made in BioRender
992 https://BioRender.com/vpa8dnh) and subsequently edited in Photoshop.

Figure 1

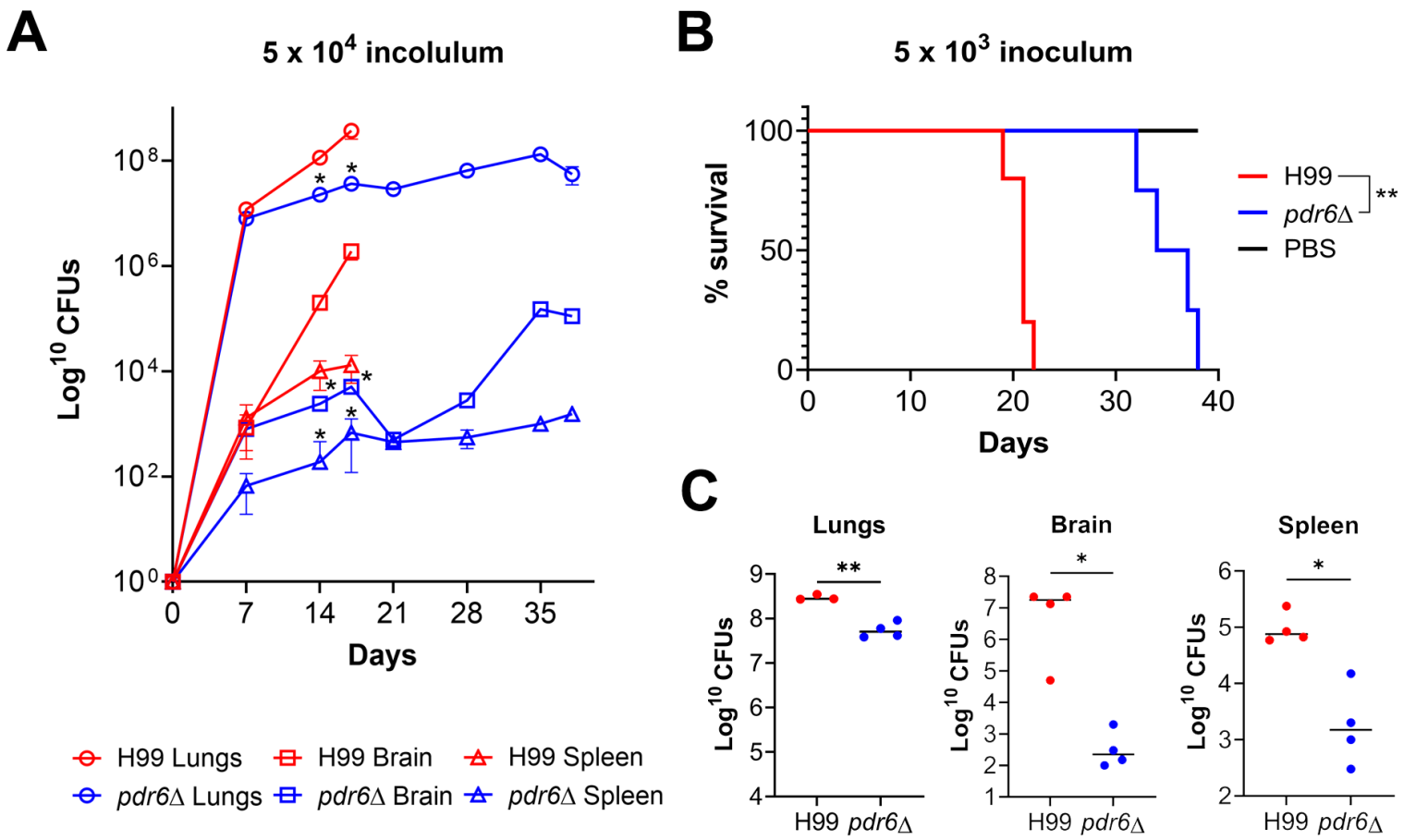
A
5 x 10^4 incolulum
Log10 CFUs
Days
H99 Lungs
H99 Brain
H99 Spleen
pdr6Δ Lungs
pdr6Δ Brain
pdr6Δ Spleen
B
5 x 10^3 inoculum
% survival
Days
H99
pdr6Δ
PBS
**
C
Lungs
Brain
Spleen
Log10 CFUs
H99
pdr6Δ

Figure 2

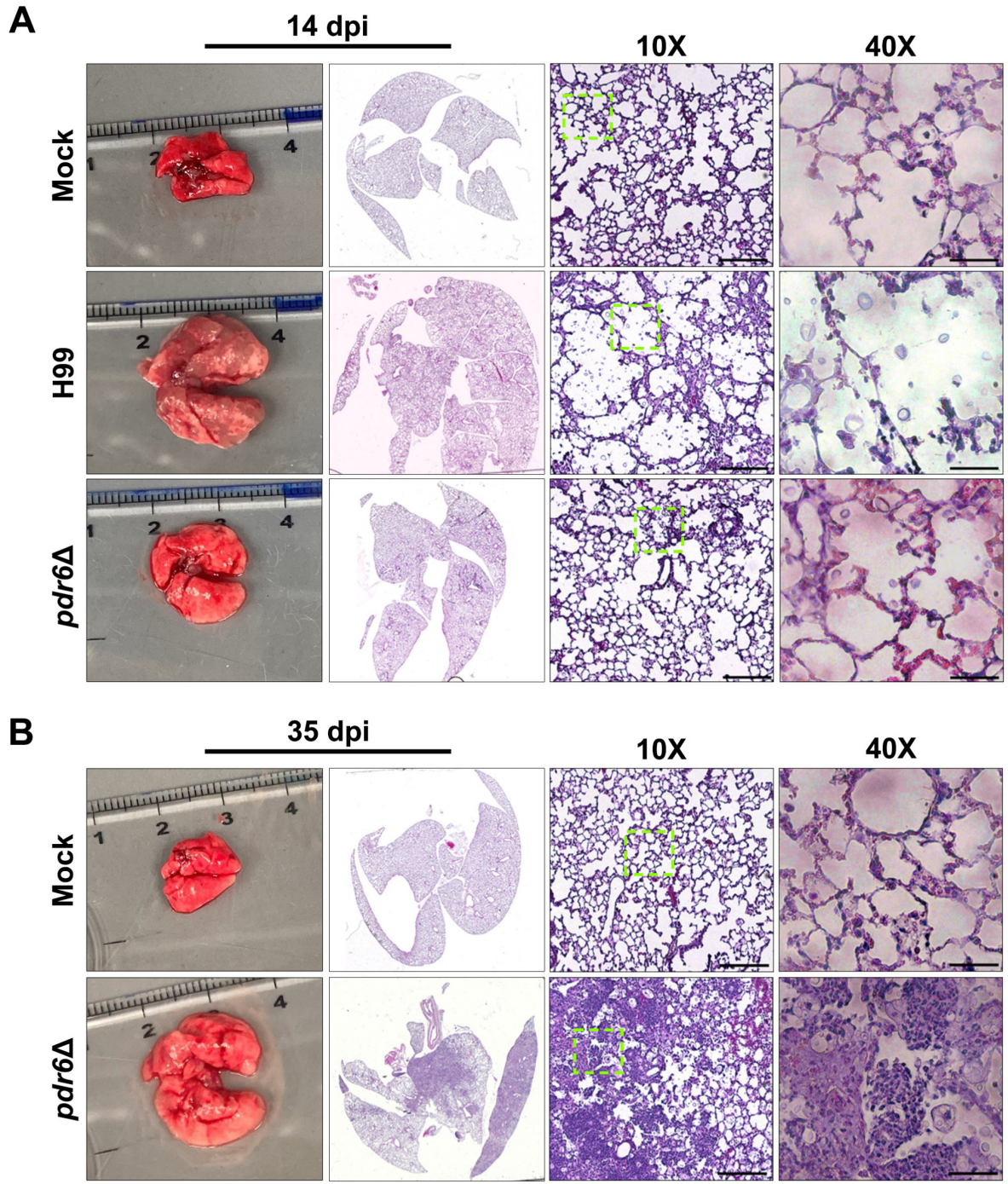

Table 1

DPI	Strain	% inflammation	Fungal infiltration	Quantitation of inflammatory immune cells/hpf 400X	Observations
7	H99	5 – 10%	20% alveoli contain encapsulated yeast	8 neutrophils 33 lymphocytes 40 histiocytes	Immune cells in peri-bronchial and perivascular space.
	*pdr6*Δ	5 – 10%	15 – 20% alveoli contain encapsulated yeast	9 neutrophils 26 lymphocytes 19 histiocytes	Immune cells in peri-bronchial and perivascular space. Some yeast has been phagocytized by histiocytes.
14	H99	10%	80 – 90% alveoli contain encapsulated yeast	52 neutrophils 26 lymphocytes 57 histiocytes	Immune cells in peri-bronchial and perivascular space.
	*pdr6*Δ	10%	50 – 60% alveoli contain encapsulated yeast	43 neutrophils 105 lymphocytes 71 histiocytes	Immune cells in peri-bronchial and perivascular space. Many histiocytes have phagocytized yeast. Areas of accumulated yeast/immune cells but no true parenchymal granulomas.
21*	*pdr6*Δ	10%	90% alveoli contain encapsulated yeast	50 neutrophils 49 lymphocytes 55 histiocytes	Immune cells in peri-bronchial and perivascular space.
28*	*pdr6*Δ	5 – 10%	80% alveoli contain encapsulated yeast	8 neutrophils 33 lymphocytes 55 histiocytes	Immune cells in peri-bronchial and perivascular space and single parenchymal granuloma (1.2mm)
35*	*pdr6*Δ	60 – 70%	100% present throughout	Too many to quantify	Consolidated parenchyma with many coalescent granulomas (histiocytes w/phagocytized yeast) and nests of neutrophils and lymphocytes with necrosis.

Figure 3

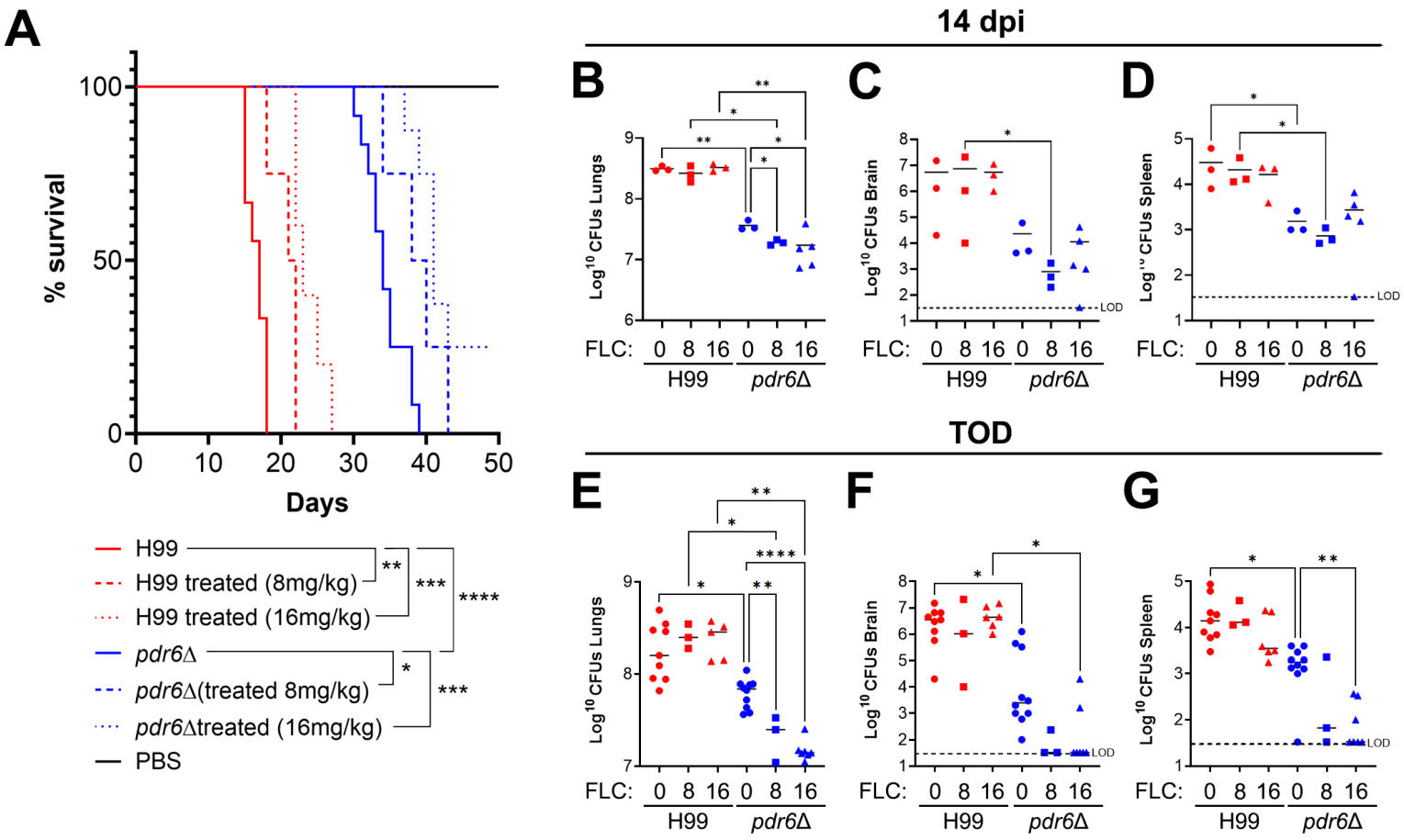
A
% survival
Days
H99
H99 treated (8mg/kg)
H99 treated (16mg/kg)
pdr6Δ
pdr6Δ(treated 8mg/kg)
pdr6Δtreated (16mg/kg)
PBS
14 dpi
TOD
B
C
D
E
F
G
Log10 CFUs Lungs
Log10 CFUs Brain
Log10 CFUs Spleen
FLC: 0 8 16 0 8 16
H99
pdr6Δ
LOD

Figure 4

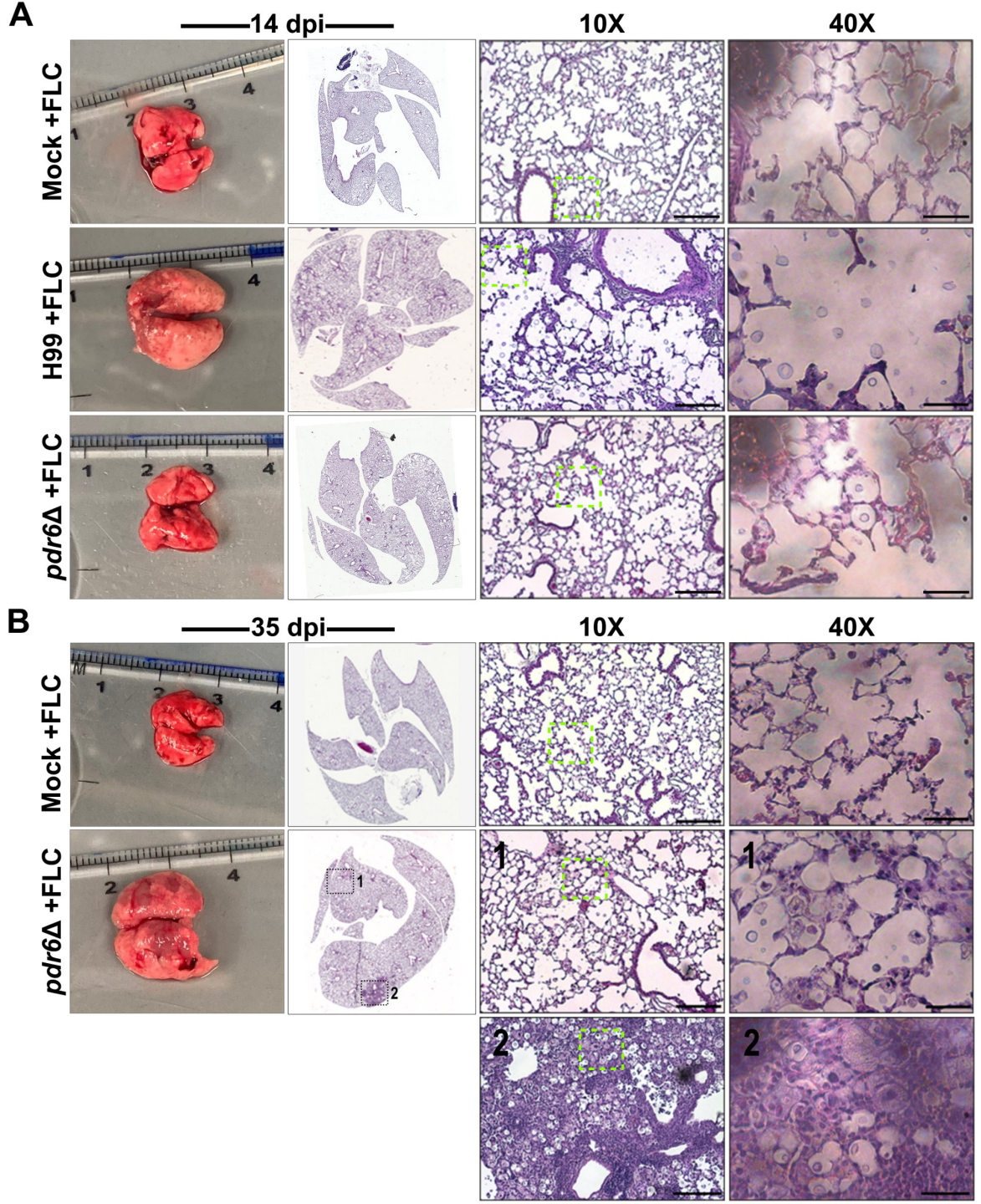
A
14 dpi
10X
40X
Mock +FLC
H99 +FLC
pdr6Δ +FLC
B
35 dpi
10X
40X
Mock +FLC
pdr6Δ +FLC

Table 2

DPI	Strain	% inflammation	Fungal infiltration	Quantitation of inflammatory immune cells/hpf 400X	Observations
14	Mock +FLC	0%	None	-	-
	H99 +FLC	5 – 10%	~ 60% alveoli contain encapsulated yeast	50 – 60 neutrophils 40 – 50 lymphocytes 15 histiocytes	Moderate number of inflammatory cells predominately present in perivascular & peribronchial areas.
	*pdr6*Δ +FLC	< 5%	30 – 40% alveoli contain encapsulated yeast	1 – 5 neutrophils 0 – 15 lymphocytes 1 – 5 histiocytes	Mild infiltrate of inflammatory cells in focal peribronchial & perivascular areas.
35	Mock +FLC	0%	None	-	-
	*pdr6*Δ +FLC	5 – 10%	45 – 50% alveoli contain encapsulated yeast	5 – 10 neutrophils 10 – 20 lymphocytes < 5 histiocytes	Mild inflammatory cell infiltrate in many peribronchial and perivascular areas. Consolidation of adjacent alveoli in solid areas.

Figure 5

And Fig. S1

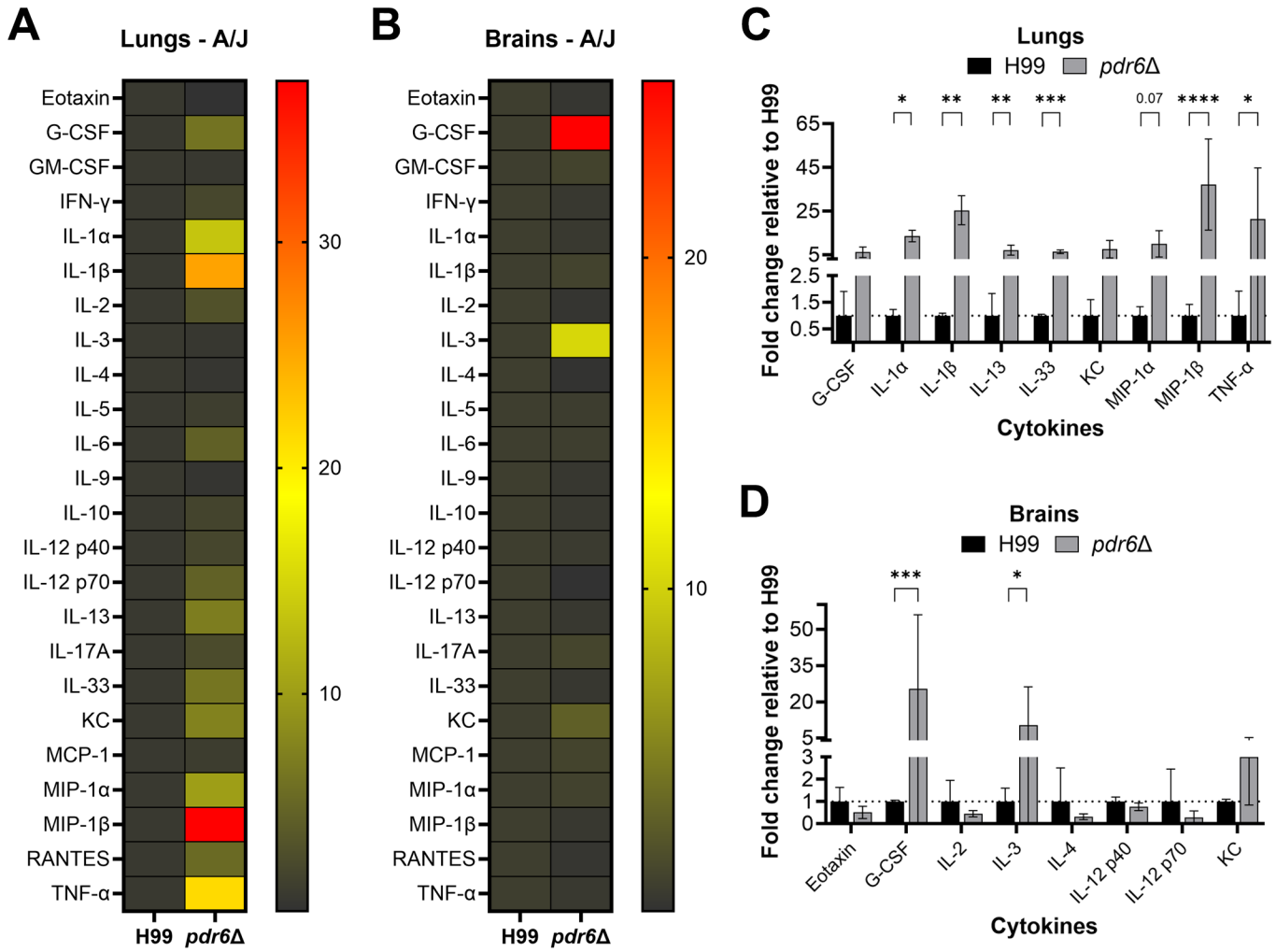

Figure 6

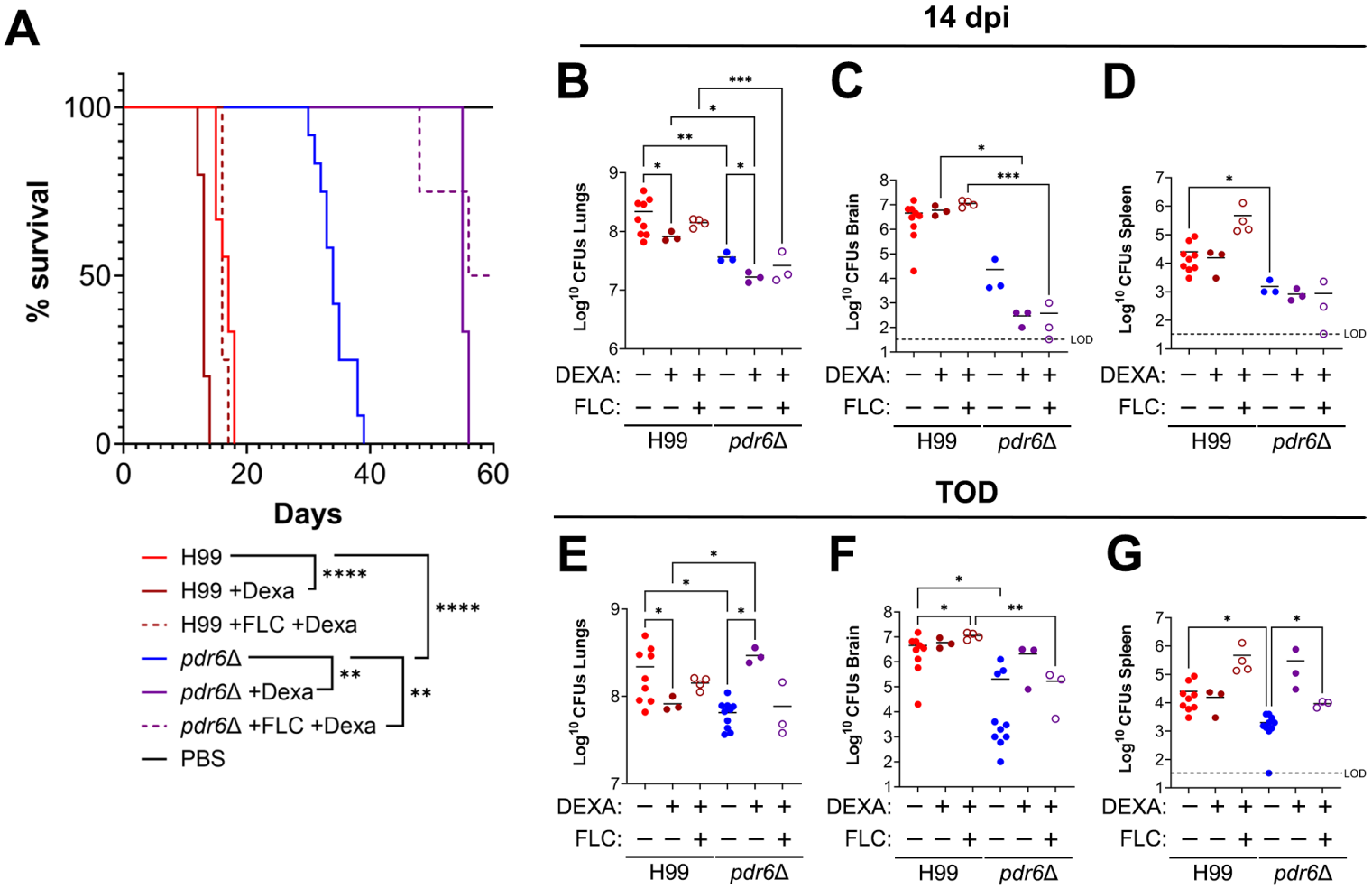
A
% survival
Days
H99
H99 +Dexa
H99 +FLC +Dexa
pdr6Δ
pdr6Δ +Dexa
pdr6Δ +FLC +Dexa
PBS
****
**
14 dpi
TOD
B
C
D
E
F
G
Log10 CFUs Lungs
Log10 CFUs Brain
Log10 CFUs Spleen
LOD
DEXA:
FLC:
H99
pdr6Δ

Figure 7

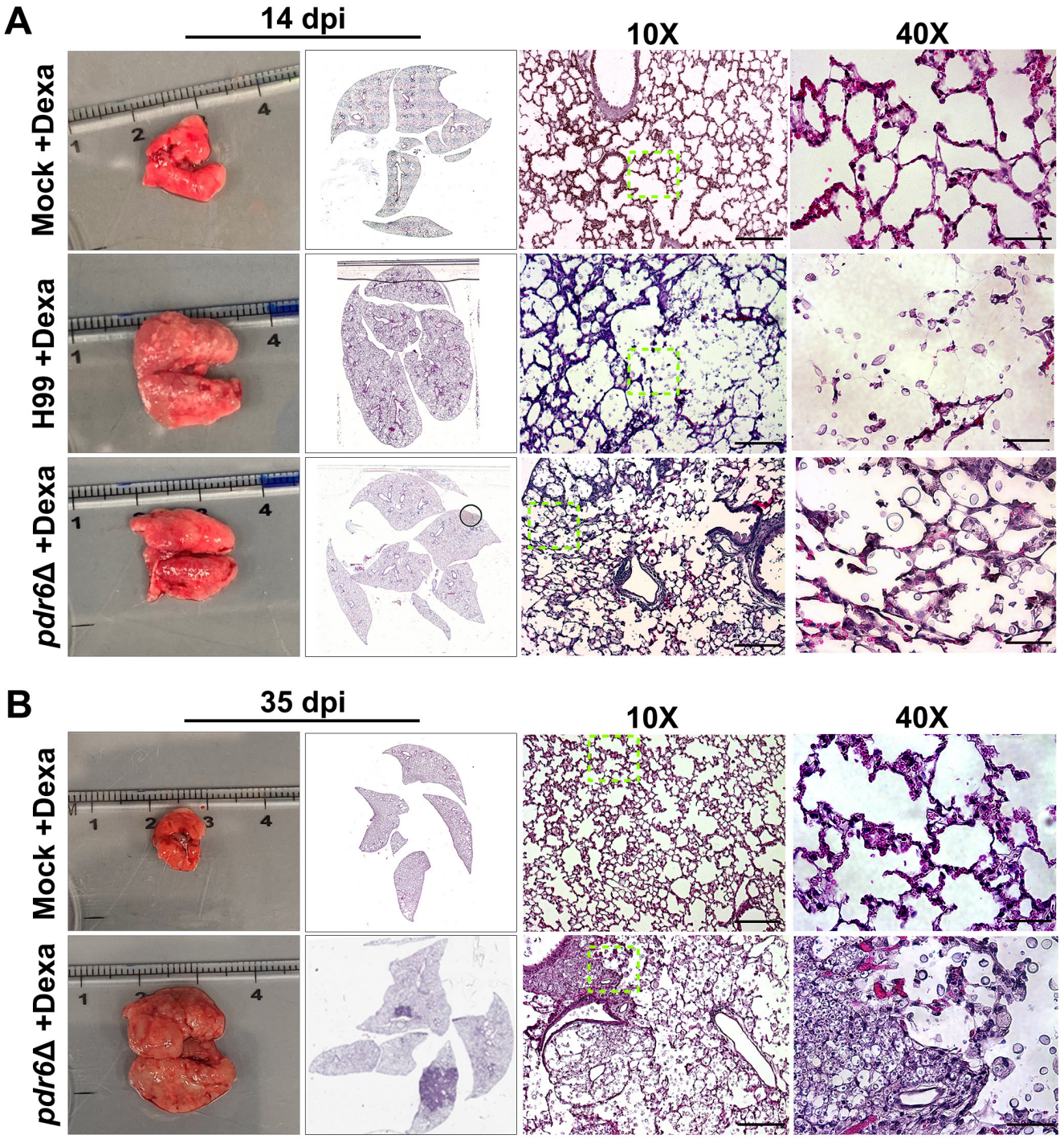
A
14 dpi
10X
40X
Mock +Dexa
H99 +Dexa
pdr6Δ +Dexa
B
35 dpi
10X
40X
Mock +Dexa
pdr6Δ +Dexa

Table 3

DPI	Strain	% inflammation	Fungal infiltration	Quantitation of inflammatory immune cells/hpf 400X	Observations
14	Mock +Dexa	0%	None	-	-
	H99 +Dexa	10%	85 – 90% alveoli contain encapsulated yeast	10 – 20 neutrophils 10 – 30 lymphocytes < 5 histiocytes	Perivascular and peribronchial aggregates of admixed neutrophils and lymphocytes.
	*pdr6*Δ +Dexa	< 5%	20 – 30% alveoli contain encapsulated yeast	5 – 10 neutrophils 5 lymphocytes < 5 histiocytes	Focal inflammatory cell nests in perivascular and peribronchial space.
50	Mock +Dexa	0%	None	-	Inflammatory cells uncommon. Rare small nests of lymphocytes on or near pleural surface.
	*pdr6*Δ +Dexa	20%	> 80% alveoli contain encapsulated yeast	5 – 10 neutrophils 5 – 10 lymphocytes 20 – 30 histiocytes	Focal consolidated areas of dense inflammatory tissue up to 4 – 5 mm in dimension.

Figure 8

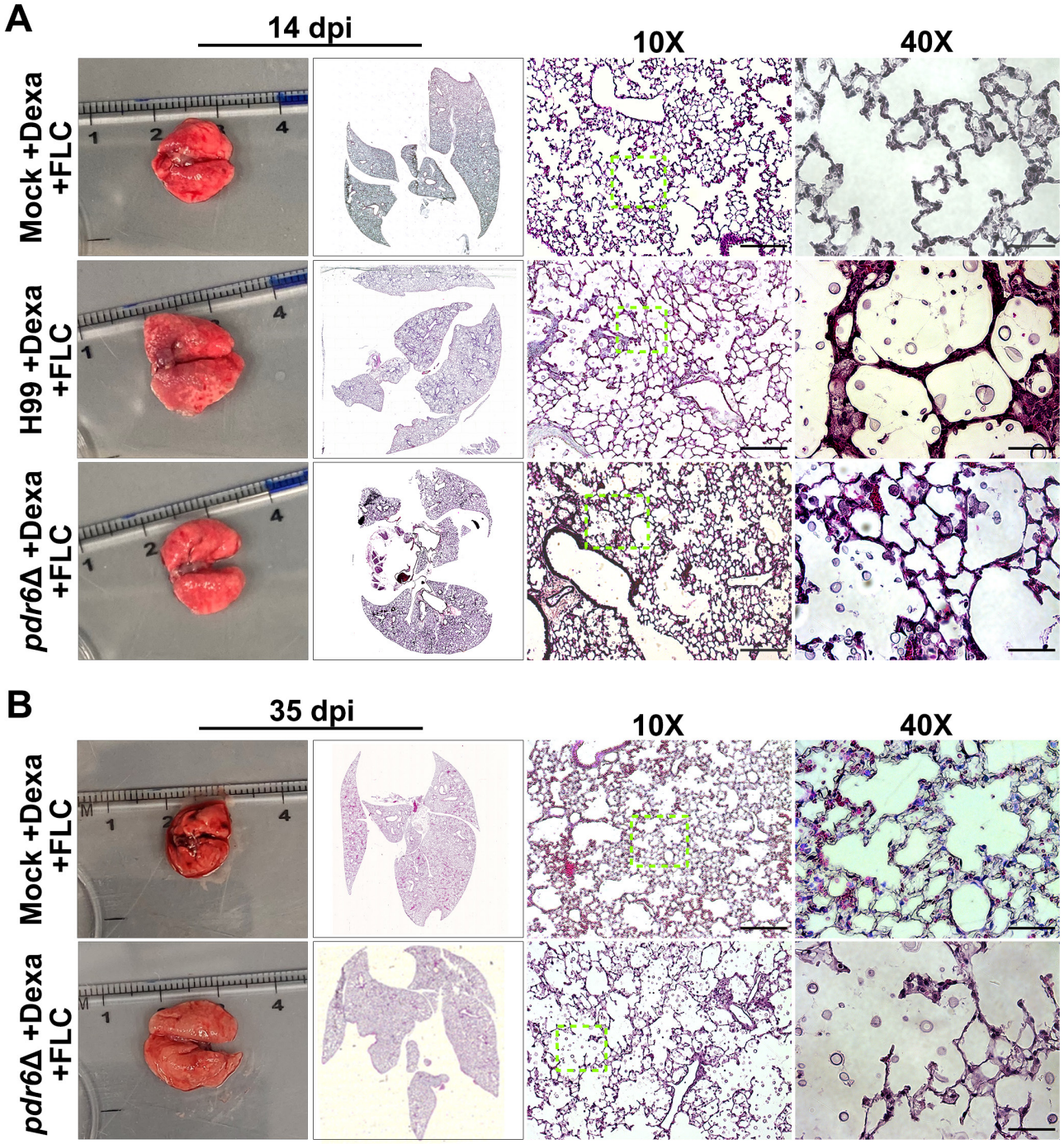
A
14 dpi
10X
40X
Mock +Dexa +FLC
H99 +Dexa +FLC
pdr6Δ +Dexa +FLC
B
35 dpi
10X
40X
Mock +Dexa +FLC
pdr6Δ +Dexa +FLC

Table 4

DPI	Strain	% inflammation	Fungal infiltration	Quantitation of inflammatory immune cells/hpf 400X	Observations
14	Mock +Dexa +FLC	0%	None	-	-
	H99 +Dexa +FLC	15 – 20%	45 – 50% alveoli contain encapsulated yeast	15 – 30 neutrophils 15 – 30 lymphocytes < 5 histiocytes	Small to medium sized nests of inflammatory cells.
	*pdr6*Δ +Dexa +FLC	0%	10 – 15% alveoli contain encapsulated yeast	-	Inflammatory cells are uncommon with rare perivascular and peribronchial nests of small lymphocytes and few histiocytes.
50	Mock +Dexa +FLC	0%	None	Rare clusters of 2 – 4 histiocytes	Mildly dilated capillaries.
	*pdr6*Δ +Dexa +FLC	0%	75 – 80% alveoli contain encapsulated yeast	-	Few small foci of perivascular lymphocytes and rare histiocytes.

Figure 9

And Fig. S2

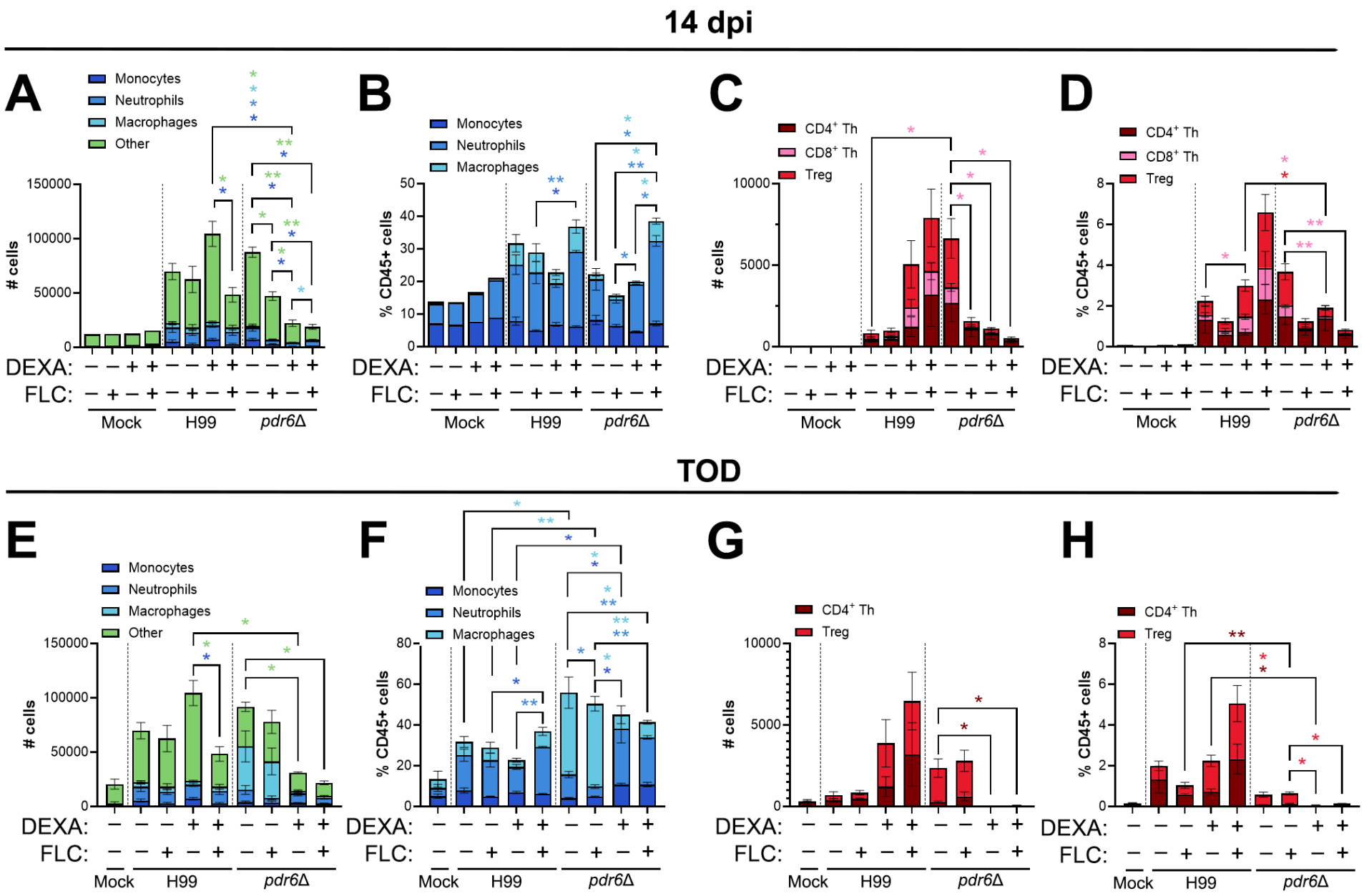

Figure 10 And Fig. S3 and S4.

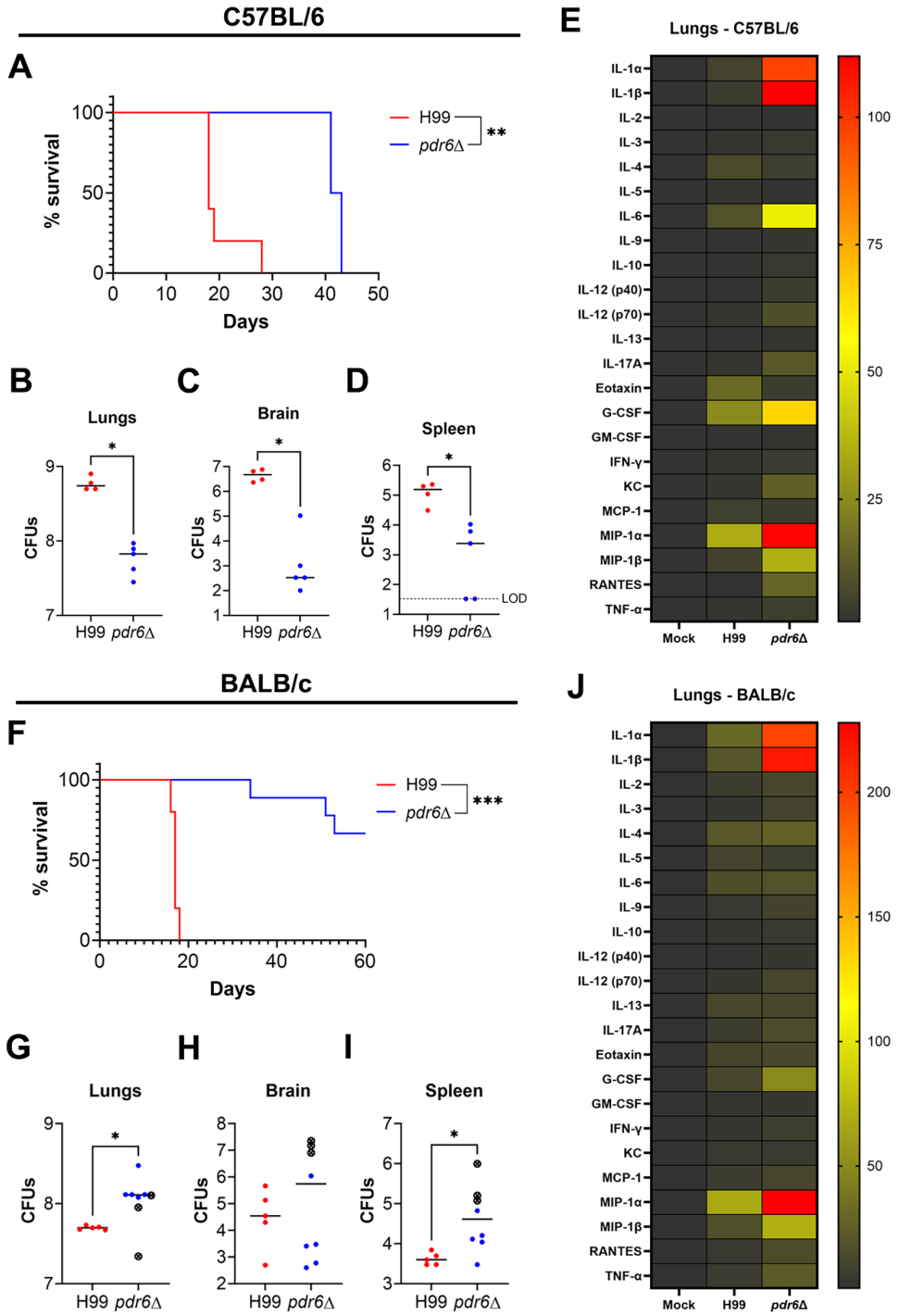

Figure 11

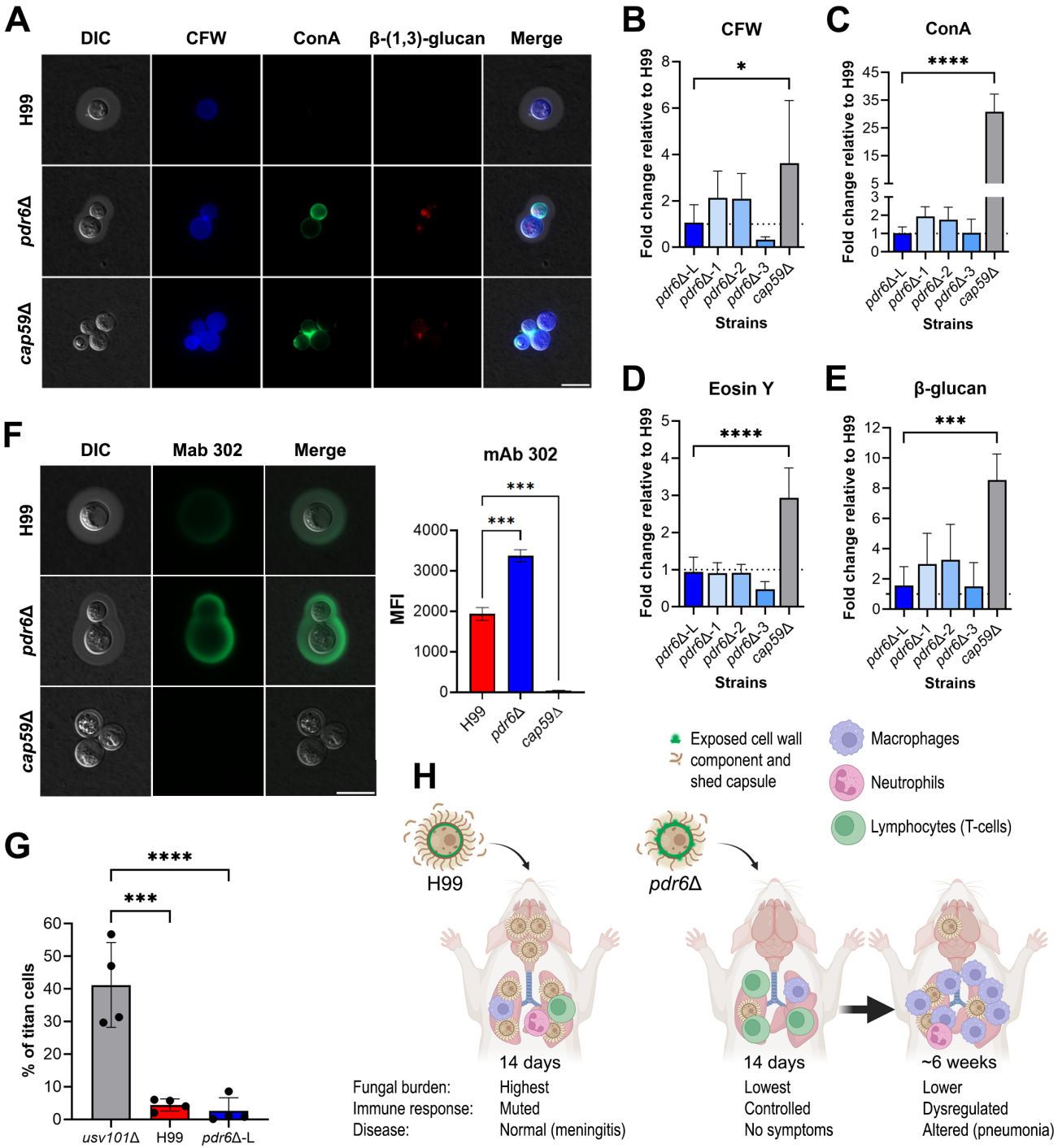
A
DIC
CFW
ConA
β-(1,3)-glucan
Merge
H99
pdr6Δ
cap59Δ
B
CFW
Fold change relative to H99
Strains
pdr6Δ-L
pdr6Δ-1
pdr6Δ-2
pdr6Δ-3
cap59Δ
C
ConA
D
Eosin Y
E
β-glucan
F
DIC
Mab 302
Merge
mAb 302
MFI
G
% of titan cells
usv101Δ
H99
pdr6Δ-L
H
Exposed cell wall component and shed capsule
Macrophages
Neutrophils
Lymphocytes (T-cells)
14 days
~6 weeks
Fungal burden:
Immune response:
Disease:
Highest
Muted
Normal (meningitis)
Lowest
Controlled
No symptoms
Lower
Dysregulated
Altered (pneumonia)

Figure S1

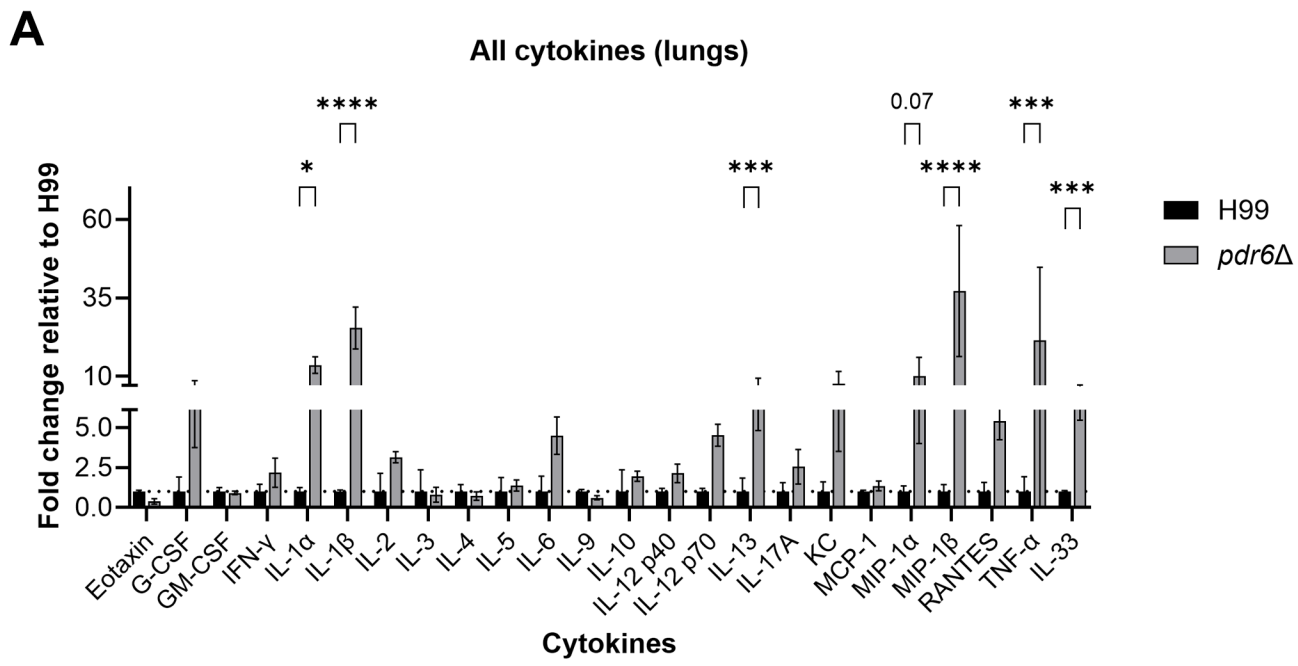
A
All cytokines (lungs)
Fold change relative to H99
60
35
10
5.0
2.5
0.0
*
****
***
0.07
****
***
***
H99
pdr6Δ
Eotaxin
G-CSF
GM-CSF
IFN-γ
IL-1α
IL-1β
IL-2
IL-3
IL-4
IL-5
IL-6
IL-9
IL-10
IL-12 p40
IL-12 p70
IL-13
IL-17A
KC
MCP-1
MIP-1α
MIP-1β
RANTES
TNF-α
IL-33
Cytokines

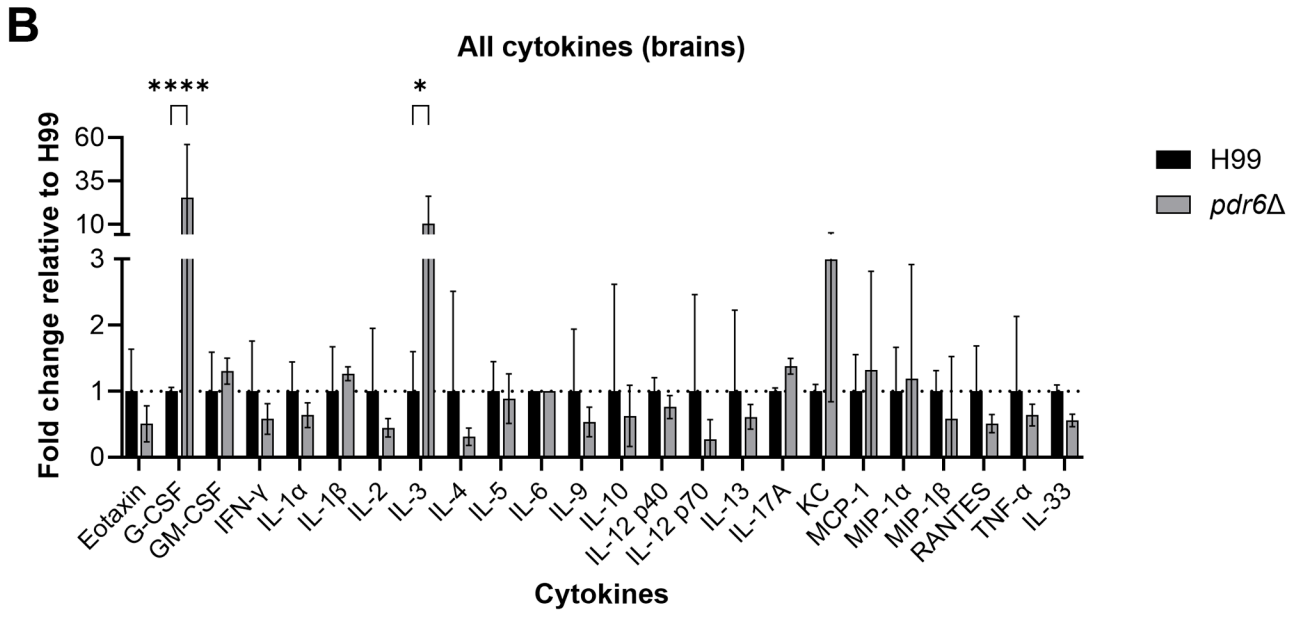
B
All cytokines (brains)
Fold change relative to H99
60
35
10
3
2
1
0
****
*
H99
pdr6Δ
Eotaxin
G-CSF
GM-CSF
IFN-γ
IL-1α
IL-1β
IL-2
IL-3
IL-4
IL-5
IL-6
IL-9
IL-10
IL-12 p40
IL-12 p70
IL-13
IL-17A
KC
MCP-1
MIP-1α
MIP-1β
RANTES
TNF-α
IL-33
Cytokines

Figure S2

Innate Immune Cell Gating Strategy

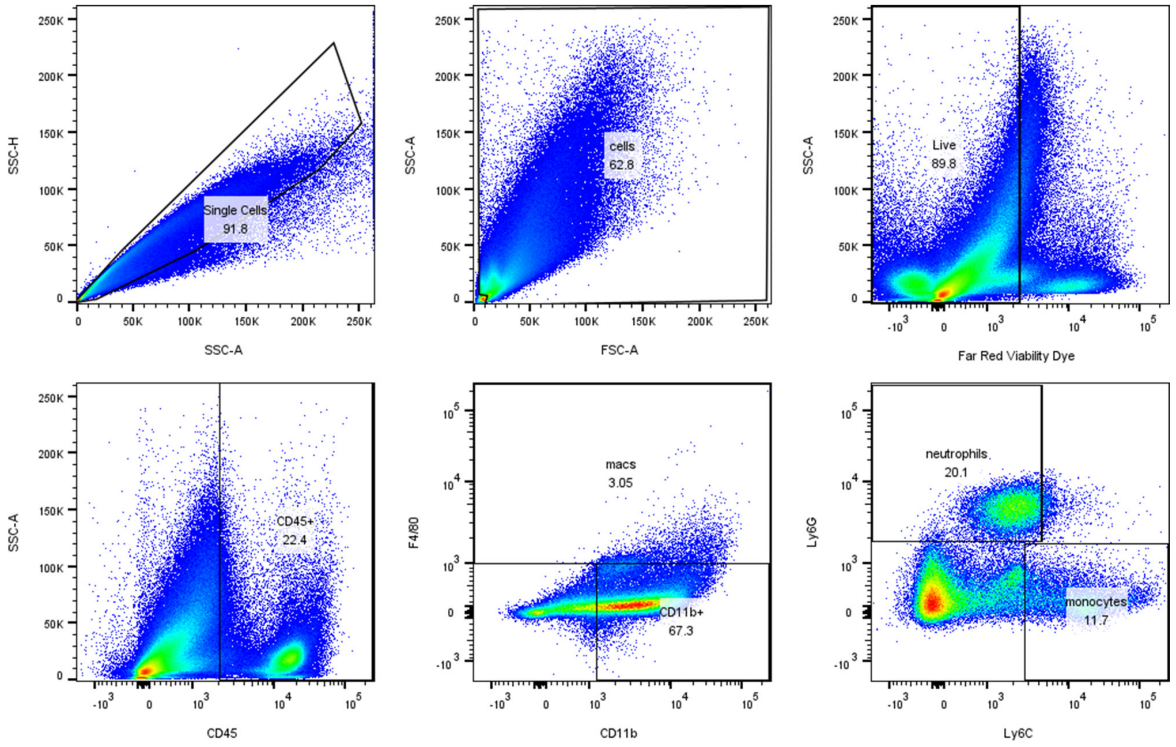

Adaptive Immune Cell Gating Strategy

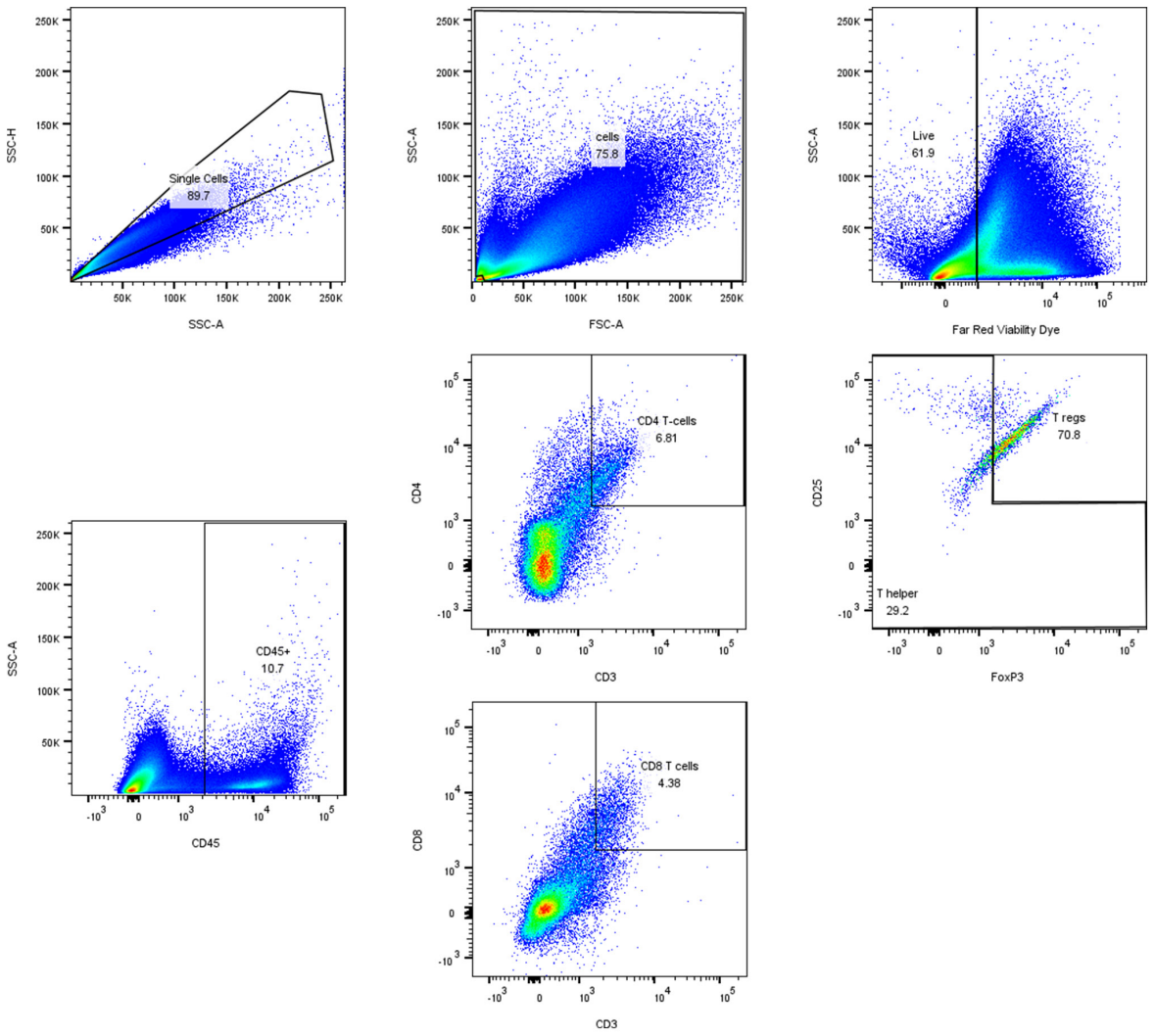

Figure S3

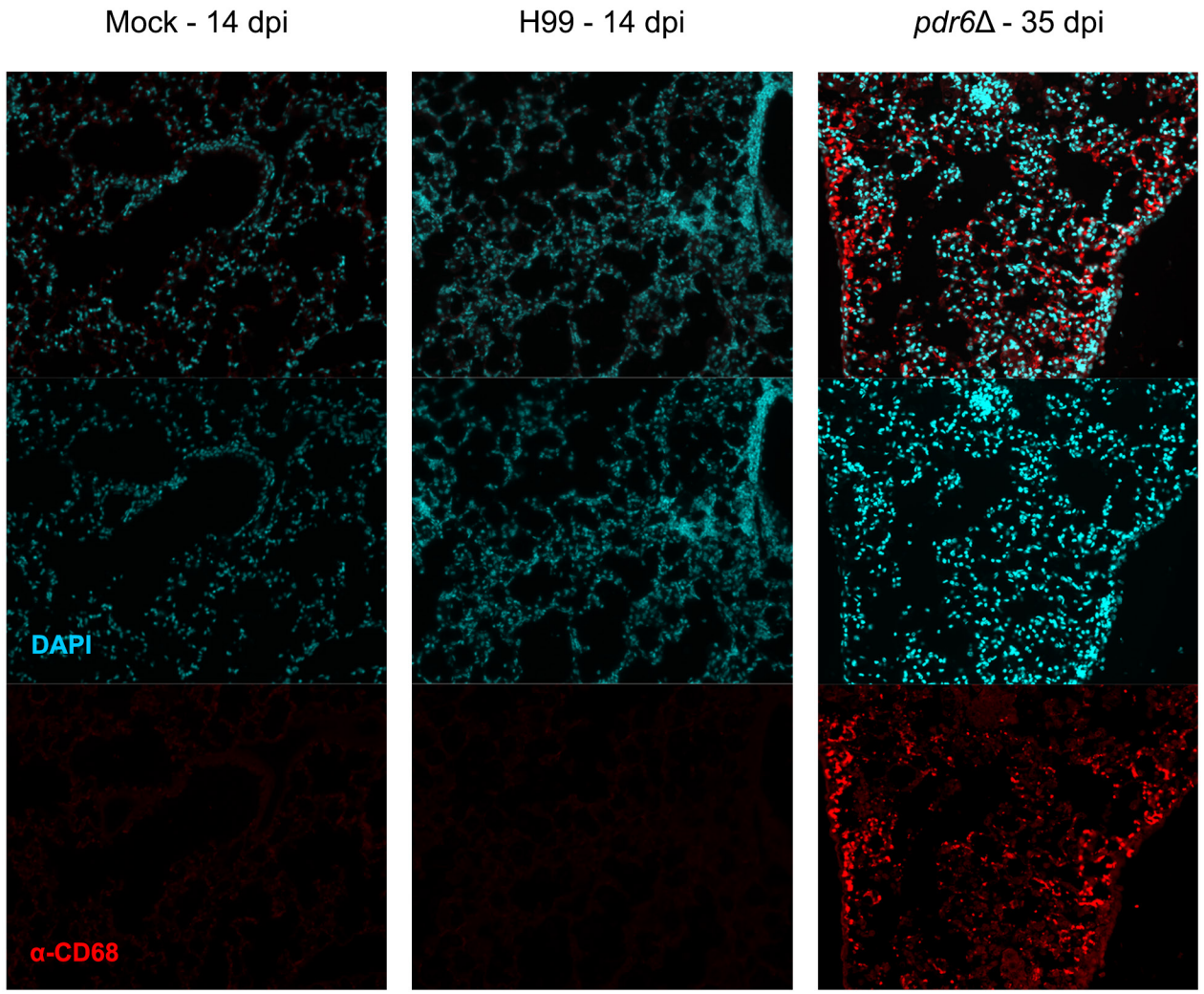

Figure S4

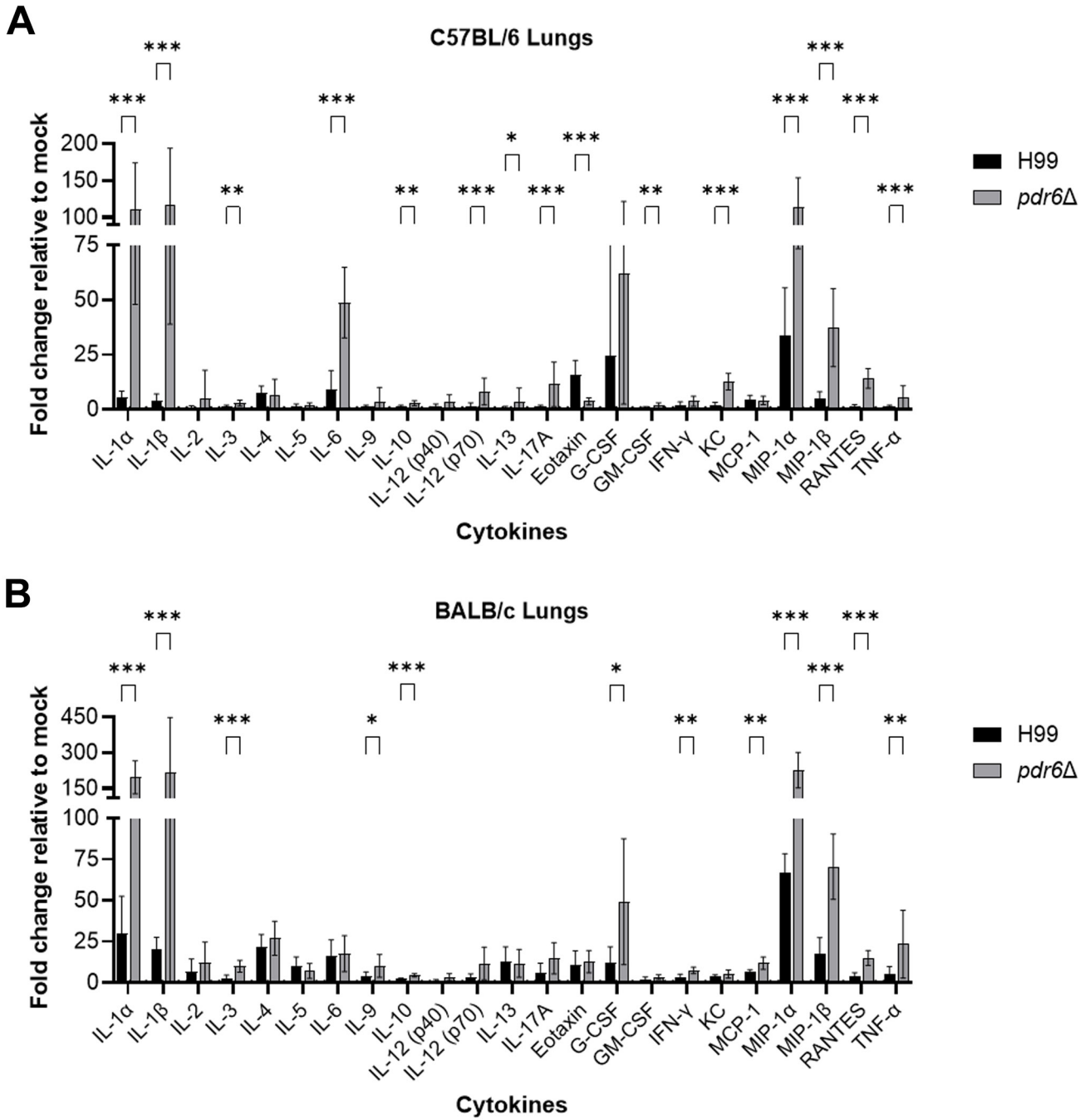
A
C57BL/6 Lungs
Fold change relative to mock
200
150
100
75
50
25
0
IL-1α
IL-1β
IL-2
IL-3
IL-4
IL-5
IL-6
IL-9
IL-10
IL-12 (p40)
IL-12 (p70)
IL-13
IL-17A
Eotaxin
G-CSF
GM-CSF
IFN-γ
KC
MCP-1
MIP-1α
MIP-1β
RANTES
TNF-α
Cytokines
H99
pdr6Δ
B
BALB/c Lungs
Fold change relative to mock
450
300
150
100
75
50
25
0
Cytokines
H99
pdr6Δ

Figure S4

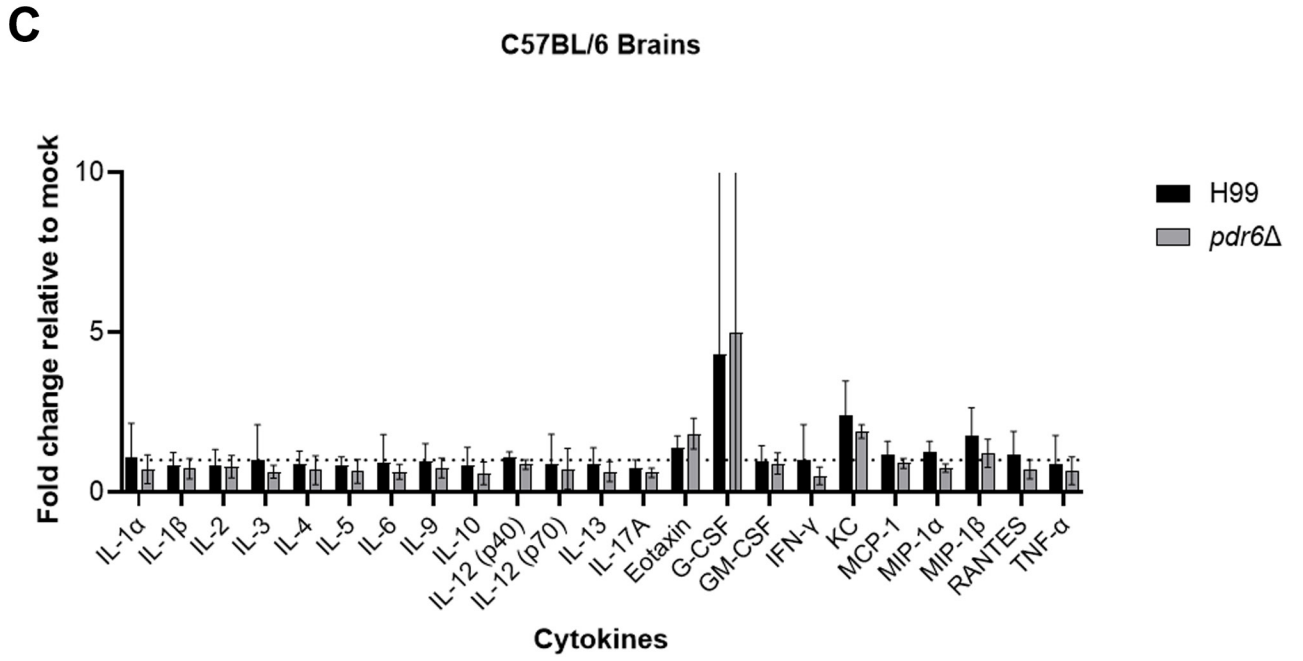
C
C57BL/6 Brains
Fold change relative to mock
10
5
0
IL-1α
IL-1β
IL-2
IL-3
IL-4
IL-5
IL-6
IL-9
IL-10
IL-12 (p40)
IL-12 (p70)
IL-13
IL-17A
Eotaxin
G-CSF
GM-CSF
IFN-γ
KC
MCP-1
MIP-1α
MIP-1β
RANTES
TNF-α
Cytokines
H99
pdr6Δ

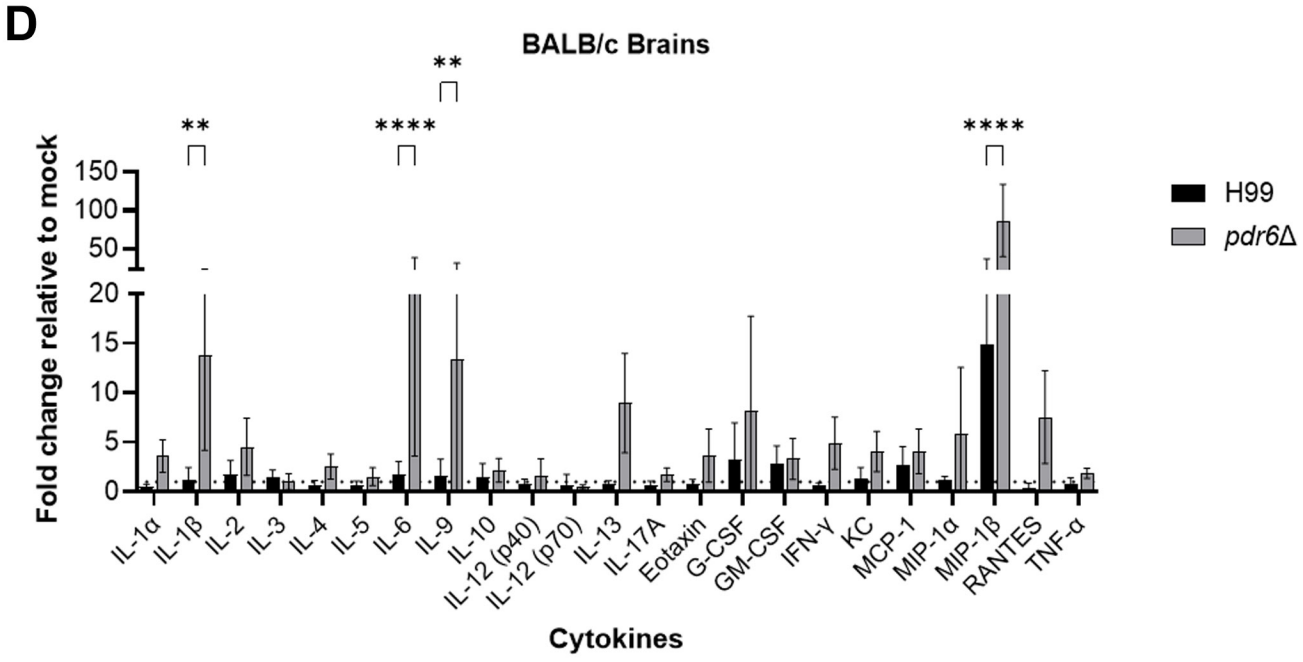
D
BALB/c Brains
**
****
**
****
Fold change relative to mock
150
100
50
20
15
10
5
0
IL-1α
IL-1β
IL-2
IL-3
IL-4
IL-5
IL-6
IL-9
IL-10
IL-12 (p40)
IL-12 (p70)
IL-13
IL-17A
Eotaxin
G-CSF
GM-CSF
IFN-γ
KC
MCP-1
MIP-1α
MIP-1β
RANTES
TNF-α
Cytokines
H99
pdr6Δ

Figure S5

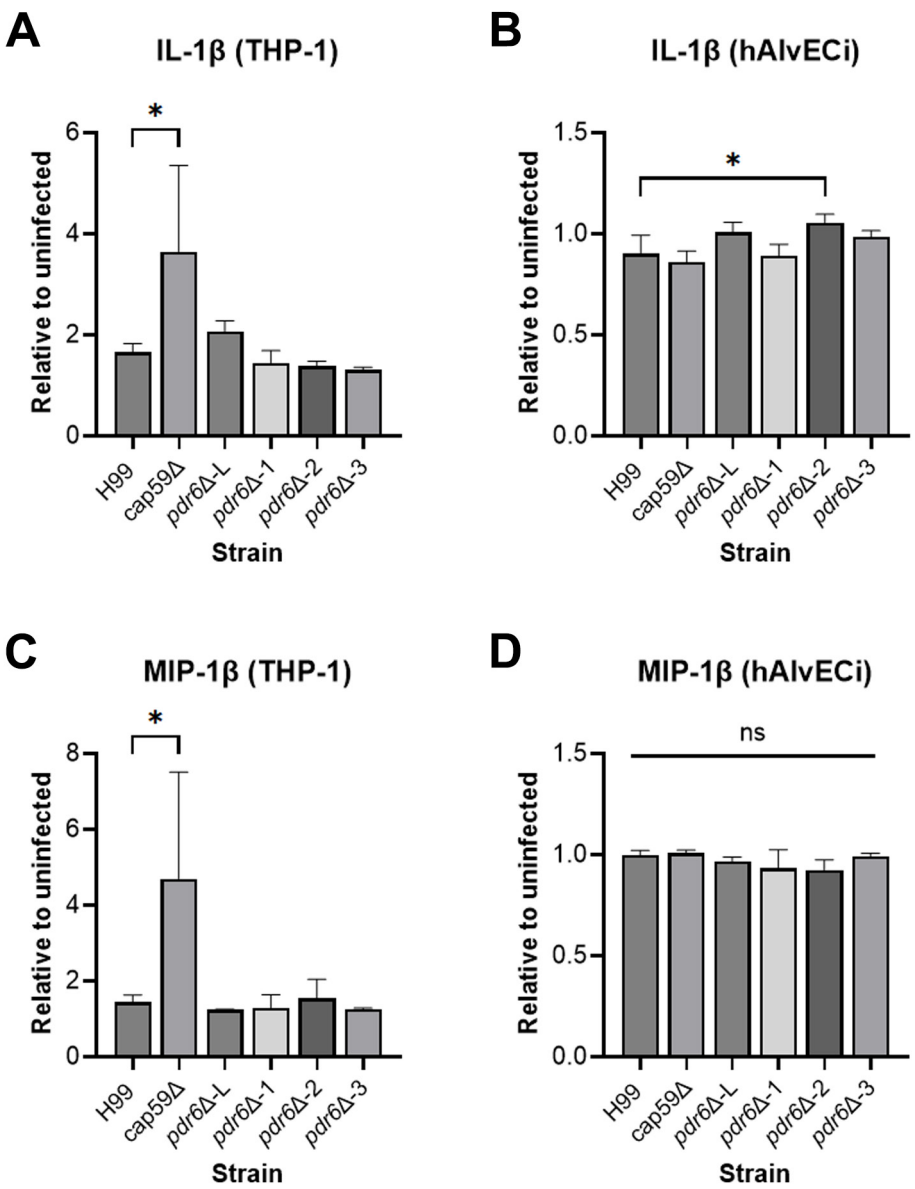
A
IL-1β (THP-1)
*
Relative to uninfected
0
2
4
6
H99
cap59Δ
pdr6Δ-L
pdr6Δ-1
pdr6Δ-2
pdr6Δ-3
Strain
B
IL-1β (hAlvECi)
*
Relative to uninfected
0.0
0.5
1.0
1.5
H99
cap59Δ
pdr6Δ-L
pdr6Δ-1
pdr6Δ-2
pdr6Δ-3
Strain
C
MIP-1β (THP-1)
*
Relative to uninfected
0
2
4
6
8
H99
cap59Δ
pdr6Δ-L
pdr6Δ-1
pdr6Δ-2
pdr6Δ-3
Strain
D
MIP-1β (hAlvECi)
ns
Relative to uninfected
0.0
0.5
1.0
1.5
H99
cap59Δ
pdr6Δ-L
pdr6Δ-1
pdr6Δ-2
pdr6Δ-3
Strain